

Modeling hydropower operations at the scale of a power grid: a demand-based approach

Laure Baratgin^{1,2}, Jan Polcher¹, Patrice Dumas³, and Philippe Quirion²

¹LMD/IPSL, École Polytechnique, Institut Polytechnique de Paris, ENS, PSL Research University, Sorbonne Université, CNRS, Palaiseau France

²CIREN, AgroParisTech, CNRS, Ecole des Ponts Paris Tech, CIRAD, EHESS, Nogent sur Marne Cedex, France

³CIRAD, UMR CIREN, F-34398 Montpellier, France

Correspondence: Laure Baratgin (laure.baratgin@lmd.ipsl.fr)

Abstract. Climate change and evolving water management practices may have a profound impact on hydropower generation. While hydrological models have been widely used to assess these effects, they often present some limitations. A major challenge lies in the modeling of release decisions for hydropower reservoirs, which result from intricate trade-offs, involving power sector dispatch, competing water uses, and the spatial allocation of power generation within the grid.

5 To address this gap, this study introduces a novel demand-based approach for integrating hydropower within the routing module of land surface models. First, hydropower infrastructures are placed in coherence with the hydrological network and links are built between hydropower plants and their supplying reservoirs to explicitly represent water transfers built for hydropower generation. Then, coordinated dam operation is simulated by distributing a prescribed electric demand to be satisfied by hydropower over the different power plants on the power grid, while considering the operational constraints associated with
10 the multipurpose nature of most dams.

To validate our approach, this framework is implemented within the water transport scheme of a land surface model and assessed with the case study of the French electrical system. We drive the model with a high-resolution atmospheric reanalysis and prescribe the observed national hydropower production as the total power demand to be met by hydropower infrastructures. By comparing the simulated evolution of the stock in reservoirs to the observations, we find that the model simulates realistic
15 operations of reservoirs and successfully satisfies hydropower production demands over the entire period. We highlight the roles of uncertainties in estimated precipitation and of the limited knowledge of hydropower infrastructure on the estimation of production. Finally, we show that such an integration of hydropower operations in the model improves the simulations of river discharges in mountainous catchments affected by hydropower.

1 introduction

20 1.1 Background and motivation

Hydroelectric power is set to play a pivotal role in ~~many of the world's numerous~~ power grids in the coming decades, ~~providing offering~~ low-carbon and dispatchable generation capacity. ~~The International Energy Agency projects a 17% increase in installed hydroelectric capacity over the 2021-2030 period (IEA, 2021). Power grids relying~~ ~~However, power grids that rely~~ on hydropower production are ~~however~~, subject to the unpredictability of weather and climate. Consequently, assessing the potential impact of drought events or climate change on hydropower production is a major concern for ~~building the development of~~ resilient energy systems. ~~Numerous studies (e.g.,~~

~~Numerous studies~~ (Lehner et al., 2005; Van Vliet et al., 2016; Turner et al., 2017; Zhou et al., 2018; Voisin et al., 2020) ~~reveal significant effects~~ ~~have revealed the significant impact~~ of climate change ~~in different geographic~~ ~~on hydropower production in certain~~ regions, including southwestern Europe and France.

~~As emphasized in the methodological review conducted by Turner and Voisin (2022), these studies commonly~~ ~~These studies typically~~ employ global hydrological models (GHMs) or land surface models (LSMs) driven by atmospheric projections generated by global climate models (GCMs) ~~They (Turner and Voisin, 2022). These models~~ simulate the regional-scale hydrological cycle, offering gridded assessments of surface runoff and streamflow, which are ~~subsequently then~~ used to derive hydropower production estimates.

However, ~~this the~~ estimation process from streamflow to hydropower production is challenging for three ~~main~~ reasons. Firstly, water can be stored in reservoirs for future use. The timing of ~~the releases is~~ ~~reservoir releases is then~~ the result of the ~~optimization of power grid management~~ ~~management of the power grid~~ and the coordinated operation of ~~plants located in different~~ ~~other plants across various~~ water catchments. Representing ~~in climate models~~ these intricate economic and spatial trade-offs, which drive the operation of hydroelectric reservoirs, ~~in climate models~~ is complex. Secondly, reservoirs that feed hydropower plants are often multi-purpose and ~~are also~~ operated to satisfy other water uses, namely irrigation or tourism. Thirdly, hydropower production can involve inter-catchment water transfers, particularly prevalent in mountainous regions where water is stored at higher elevations before being channeled to power plants located in the valleys. Representing these short-scale processes within regional models poses further complications.

Existing studies adopt diverse strategies to represent these complex operations of hydroelectric reservoirs, which are generally categorized into two main approaches (Nazemi and Wheeler, 2015b).

On the one hand, simulation algorithms rely on predefined rules to compute ~~daily or monthly~~ reservoir releases. These rules are often a function of reservoir inflow and filling level ~~inspired by the pioneering work of Hanasaki et al. (2006)~~ ~~They generally do not consider the reservoir's specific purpose, except for irrigation-aimed reservoirs, the release rules of which also depend on downstream irrigation demands. Hydropower and flood control reservoirs are therefore represented identically, including in models such as (e.g. in~~ MOSART-WM ~~a reservoir scheme used for many recent studies focusing on hydropower (Zhou et al., 2018; Voisin et al., 2020; Ralston-Fonseca et al., 2021). However, Abeshu et al. (2023) demonstrate that, in practice, the operation of hydropower reservoirs differs from that of flood control reservoirs. One significant distinction~~

is that hydropower reservoirs are operated with the intention of maximizing the water level in the reservoir at the moment of release, leveraging a high head, while flood control reservoirs are drained preemptively to avoid potential flood events. The realism of the operations simulated in models that do not distinguish hydroelectric reservoirs can therefore be questioned. Alternatively, the rules can be by Zhou et al. (2018); Voisin et al. (2020); Ralston Fonseca et al. (2021)) or defined based on target curves, which set daily target water levels and determine releases accordingly. This approach is utilized, for example, in Vic-Res (Dang et al., 2020), which is employed in some hydropower studies (Chowdhury et al., 2021; Siala et al., 2021). This of water levels from which the release is determined (e.g. in VIC-RES (Dang et al., 2020) used by Chowdhury et al. (2021); Siala et al. (2021)). Such a method accounts for the seasonal behavior of hydropower reservoirs, such as drawdown during drier months and recharge during the monsoon season, hydroelectric reservoirs, but it misses the representation of short-term operational constraints.

operations, as no links with the power system needs are made. On the other hand, optimization algorithms based on the pioneering work of Haddeland et al. (2006) determine the optimal release for each dam. The objective function to optimize varies depending on the reservoir's primary purpose, aiming to maximize individual production for hydropower reservoirs. One limitation of this approach is the requirement of future inflow knowledge for each reservoir over the optimization horizon, necessitating multiple runs of the model to optimize reservoir releases. More recent models utilize stochastic dynamic programming (SDP) approaches to account for the uncertain nature of reservoir inflows (Turner et al., 2017). In these models, monthly releases are determined at each time step to maximize the total expected production by hydropower, considering both immediate and future production. hydroelectric reservoirs. However, these methods consider each reservoir independently and often employ large time steps (monthly) to reduce computational strain.

When the models distinguish the different usages differentiate the various uses of reservoirs, they classified-categorize the reservoirs based only-solely on their primary purpose (Abeshu et al., 2023), which. This approach does not allow for the representation of all the constraints applying that apply to most hydroelectric reservoirs, that are often dedicated to other purposes as well which are often multi-purpose. Moreover, none of these studies operate the dams as a network that takes advantage of the spatial complementarity of climatic regions or cascading effects.

Finally, to our knowledge, none of these large-scale studies explicitly model the water transfers from reservoirs to power plants. In most cases, they employ the flow rate within the grid cell corresponding to where the power plant to deduce is located is used to estimate its production, without considering the actual reservoir location location of the reservoir (Van Vliet et al., 2016; Zhou et al., 2018; Voisin et al., 2020). However, this approach can potentially may lead to an overestimation of production, given that the flow as the flow rate at the plant site is necessarily greater than that at the greater than at an upstream dam site, and inter-basin transfers may also occur.

1.2 Objectives

The objective of our this study is to present the original methodology we developed to estimate hydropower production at the scale of a regional power grid. This methodology is based on the simulations of a GHM or LSM, answering and addresses the three challenges previously identified: (i) considering the coordinated management of the entire power system at the scale of the

~~regional power~~ grid; (ii) accounting for ~~the~~ multi-purposes objective of reservoirs that store water for hydropower production; (iii) representing the inter-catchment water transfers from reservoirs to power plants.

Our approach is inspired by the demand-based algorithms used for irrigation reservoir management, pioneered by Hanasaki et al. (2006). In these algorithms, a demand point (irrigated area) is connected to a supply point (river), with the water demand of the downstream irrigated area driving upstream reservoir releases (~~Nazemi and Wheeler, 2015b~~). ~~Zhou et al. (2021) developed such a module to operate irrigative reservoirs in the ORCHIDEE (ORganizing Carbon and Hydrology In Dynamic EcosystEm) land surface model (Krinner et al., 2005) framework, which was validated for the Yellow River basin. In these algorithms, the irrigative demand input is inferred based on withdrawal observations or model estimations. (Nazemi and Wheeler, 2015b; Zhou et al., 2021)~~

In our methodology, hydropower plants are linked to reservoirs whose ~~release depends~~ releases depend on the demand for hydropower production ~~addressed to the plant. This local "hydropower demand" derives from the decisions of power system dispatch made at the grid level. We assume that this hydropower demand results from the decisions of a social planner in charge of the dispatch of.~~ At the geographical scale of the power demand to whole power grid, the balance between electricity demand and generation is the primary concern, regardless of the various available electricity sources. The social planner knows the potentials and costs of all the units available in the network area, as well as the electricity demand, and calls the appropriate source when the notional price of electricity corresponds to the unit opportunity cost specific locations of consumption and generation. Consequently, we assume that all hydroelectric reservoirs in the power grid may contribute to satisfying the demand for dispatchable hydropower production defined at the grid level, as a result of the power system dispatch decisions. Power dispatching involves deciding which types of power plants are activated to satisfy the total power demand, based on the cost and availability of generation resources. We do not explicitly represent this side of the ~~electricity power~~ system decisions but ~~assume~~ corresponding "hydropower demand" consider a corresponding demand for dispatchable hydropower to drive the ~~operations of hydropower operation of the hydroelectric~~ reservoirs in our model. ~~At the scale of the power grid, the balance between power demand and generation is the primary concern, regardless of the specific locations of consumption and production sites.~~ Therefore we consider an aggregated hydropower demand that needs to then be fulfilled by the different plants within the grid.

We implement ~~our~~ the proposed methodology in the ORCHIDEE LSM (~~Krinner et al., 2005~~), but it aims to be usable in ~~all LSMs and GHMs~~ any LSM or GHM. The first steps of building a river network that represents inter-catchment hydropower transfers and defining rules for reservoir releases are generic and only require basic information on dam and plant characteristics. To validate the effectiveness of the approach, we apply it to the French power grid, ~~which heavily relies on hydropower, accounting for approximately 10% of its production.~~ A calibration step is added, which requires more information on individual plants to adjust the efficiencies of the power plants. Finally, simulated and actual operations of ~~hydropower hydroelectric~~ reservoirs are compared.

The paper is structured as follows: Sect. 2 describes the proposed methodology and its originality. Sect. 3 introduces the data and methods used for our case study of the French power grid and assesses the performance of ORCHIDEE in reproducing river discharges over this area. Sect. ~~2.5 estimates and discusses the production biases of the model in the case study and~~

~~presents the calibration method we use to address them.~~ Sect. 4 details the modeling results, and finally Sect. 5 discusses these results and concludes by outlining future perspectives of research.

2 ~~Presentation of the modeling approach~~ Model

125 Our method relies on three main novelties: building a river network that includes most hydropower-related infrastructures and represents inter-basin hydropower transfers (Sect. 2.1), implementing a reservoir scheme that accounts for multi-purpose reservoirs (Sect. 2.2), and using hydropower demand to infer ~~hydropower-hydroelectric~~ reservoir operations (Sect. 2.3).

2.1 Definition of a routing network that includes hydropower connections

2.1.1 General principles

130 ~~ORCHIDEE is a LSM, initially designed to be coupled to an atmospheric global circulation model (Krinner et al., 2005). In this study, we use it in stand-alone mode, forced by an atmospheric forcing dataset.~~

~~The typical~~ The spatial resolution of LSMs is imposed ~~GHMs or LSMs is typically constrained~~ by the atmospheric grid of the forcing files, ~~generally from which is generally set at~~ 0.5° (around 50km approximately 50 km) for large-scale implementations ~~to and~~ 0.1° (around 10km approximately 10 km) for regional implementations. However, human activities such as irrigation or
135 urban areas operate at much higher spatial ~~resolution~~ resolutions, typically within a few kilometers. The concept of hydrological transfer units (HTUs) has been introduced in routing modules to bridge the gap between ~~such differences in the differing~~ resolutions of atmospheric and hydrological processes resolutions and to provide the opportunity to incorporate human activities in such models (~~Nguyen-Quang et al. (2018) for ORCHIDEE model~~) (Nguyen-Quang et al., 2018). HTUs correspond to sub-grid river basins ~~which allow the~~, which permit runoff generated in one atmospheric grid cell to flow into multiple neigh-
140 boring atmospheric grid cells. ~~These smaller units allow for a better~~ The introduction of these smaller units allows for a more accurate representation of the river system and its interaction with human activities, including hydropower.

Three types of hydropower plants are distinguished, with different implications on locations:

- ~~Run-of-river plants~~ Run-of-river plants lack any storage capacity and generate electricity ~~accordingly~~ according to the instantaneous river discharge at the plant location. There is no difficulty involved in the location of the plants;
- 145 – ~~Reservoir plants~~ Reservoir plants are fed by reservoirs ~~which that~~ can store a specified water volume and are often also used for other purposes, which may constrain the operations of the plant. Electricity production does not necessarily take place at the location of water storage, therefore the plant and the reservoir need to be located separately.;
- ~~Pumped-hydro-storage (PHS) plants are able to pump water from a downstream reservoir to an upstream one during low electric demand periods. The links with both downstream and upstream reservoirs needs to be determined.~~ Poundage
150 plants are defined in some regions as a subcategory of reservoir plants whose upstream reservoir is relatively small and only allows to store water for a short period.

As an example of different locations of reservoir and power plant, the ~~power plant of "La Bathie" -power plant~~, the largest reservoir power plant in France ~~-uses water from-~~, draws water from the Roselend reservoir, which is located about 20 km away (see D). At a kilometric resolution, this implies horizontal water transfers between these two locations (water withdrawal and restitution) ~~that cannot be merged, as has been done in previous studies (Zhou et al., 2018).~~ This, which requires the reconstruction of the hydroelectric water supply network within the routing network of ORCHIDEE.

We proceed in three steps as illustrated in Fig. 1. First (Fig. 1-b), we place dams and hydropower plants on a high-resolution river network (MERIT (Yamazaki et al., 2019) is used in this study), based on geo-referenced data and upstream area provided in ~~the infrastructure~~ infrastructure databases. The location procedure is detailed in Appendix A and the ~~infrastructures infrastructure~~ datasets used for our study of France are presented in Appendix B. Then, we build the adduction network by identifying supposed connections between power plants and dams that feed them (see ~~Sect. ?? Appendix A~~ for more details on the procedure to build the adduction network). Finally (Fig. 1-c), we form HTUs by aggregating MERIT pixels in an atmospheric grid cell with the same general flow direction following the procedures described in Nguyen-Quang et al. (2018) and Poleher et al. (2023) Nguyen-Quang et al. (2018) and Polcher et al. (2023).

This aggregation procedure results in an HTU network representing natural and human-made water flows. It can be seen as a directional graph (Fig. 1-d) where vertices correspond to HTUs and edges represent directional water flows (natural and human-made for hydropower purposes). Considering this graph, hydropower plants are placed on the edges connecting the HTU of their withdrawal point and the HTU downstream of the one in which they are located. Fig. 2 introduces the notation that will be used throughout the article to index HTU-HTUs and edges in such graphs. It shows that the water used to produce electricity can follow a different path to-from the natural flow out of the reservoir. This approach allows for the representation of this distinction independently of the atmospheric resolution.

2.1.1 Adduction network

~~Reservoir and PHS plants produce power from water releases from upper reservoirs. To explicitly represent this adduction network in our model, we have to identify such connections between a feeding reservoir and a power plant. For each reservoir or PHS plant, we thus select as feeding reservoir the one that maximizes the potential function $\phi = \frac{U*V*h}{d}$, where U is the upstream area of the dam, V is the storage capacity of the reservoir, h is the elevation difference between the plant and the reservoir and d is the horizontal distance between them. Similarly, a downstream reservoir is selected for each PHS plant by maximizing $\phi^l = \frac{U*V*(-h)}{d}$. The definition of these potential functions is inspired by similar works aiming to connect an irrigative area to a water supply point (Neverre, 2015; Zhou et al., 2021).~~

~~This position algorithm relies on the assumption that each plant is fed by only one reservoir. This assumption is however debatable, especially for plants in mountain areas that may be connected to several reservoirs. In this case, our choice of potential function ϕ privileges the reservoir with the largest upstream area since it is likely to determine the production potential of the plants. During calibration (see Sect. ??), plants for which the identification of a single reservoir conducts to a significant misrepresentation of the plant's hydropower potential are identified and a correction is made by moving the withdrawal point so that it gathers enough water to ensure the observed production is possible.~~

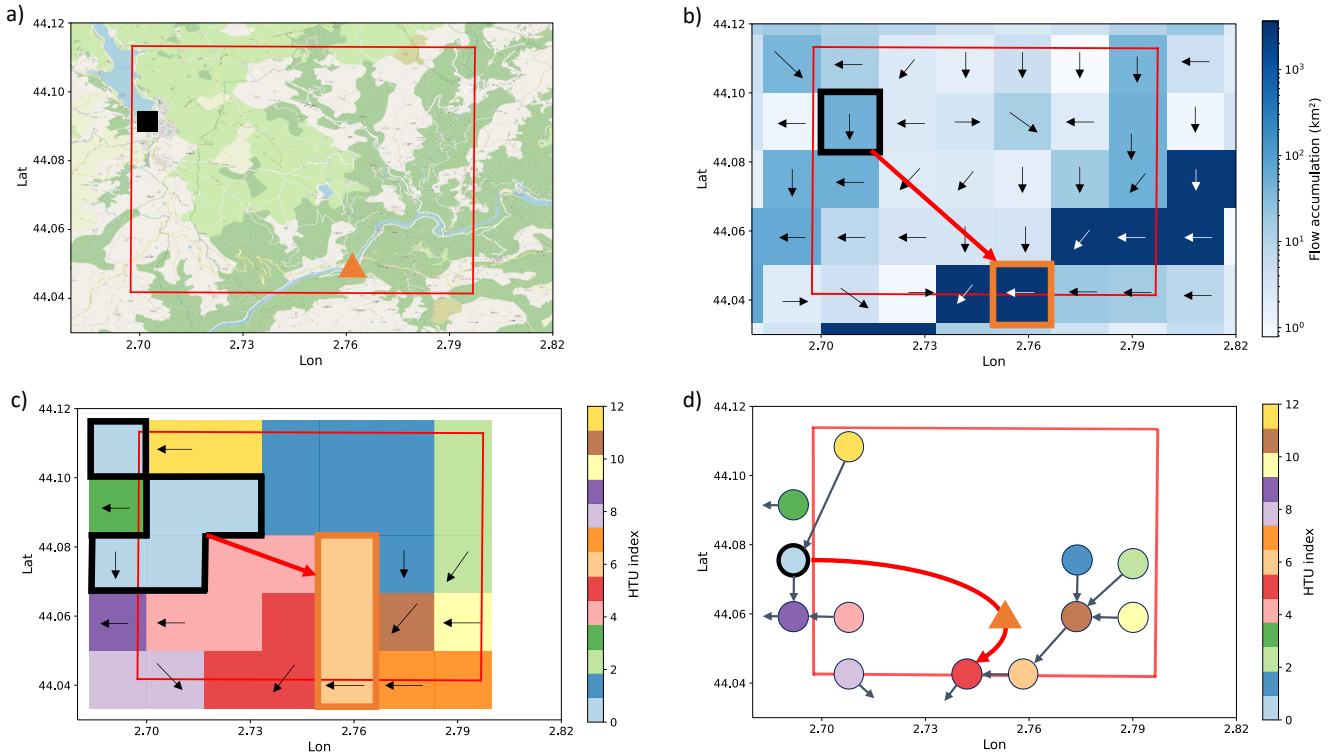


Figure 1. Illustration of the procedure to build ORCHIDEE routing network with the example of Pouget hydropower plant in France. (a) Geographic context of Pouget power plant (orange triangle) and its feeding reservoir (black square indicating the location of the dam). **Red-The red** grid indicates the atmospheric grid. (b) Flow directions and accumulation for the MERIT pixels overlapping the atmospheric grid. MERIT pixels in which we located the power plant and the dam are respectively indicated in orange and black while the red arrows represent the adduction network link we identify. (c) Resulting HTUs decomposition. The location of the infrastructures is reported in the corresponding HTUs (d) Corresponding HTUs graph. The HTU containing the dam is indicated with a bold black outline while the power plant (orange triangle) is placed on the edge between the reservoir and the HTU downstream from the one in which it has been located.

2.1.1 Aggregation to form the HTUs

Attributes and variables describing reservoir and hydropower characteristics of each HTU i and vertex (i, j) are presented in Table 1.

190 **Note that each vertex and edge can respectively contain only one dam or hydropower plant. If several reservoirs are placed on the same HTU during pixels aggregation, their respective volumes for the different uses are summed. If two plants are placed on the same edge, their installed power and pumping capacity as well as their head are summed only if both plants have the same input point. Otherwise, only the plant with the highest installed capacity is kept. As in other studies (Abeshu et al., 2023), all the reservoir attributes are associated with the HTU of the dam (even if its water surface can be larger than the HTU area and its geometry is different from the HTU geometry).**

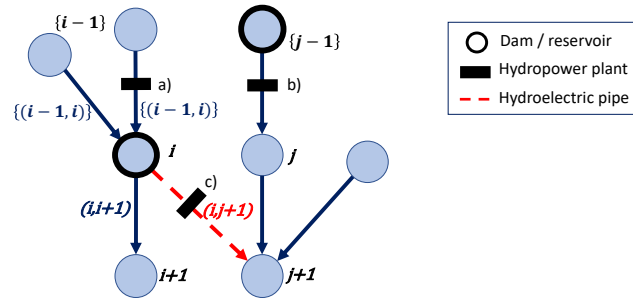


Figure 2. Graph representation of the river routing network built. Each vertex represents an HTU. HTUs containing a dam are represented by bold dark circles. Edges represent existing water flows-flow directions (blue edges for natural water flows and dashed red ones for hydroelectric pipes). Power plants are placed on edges whose water flows they can use to produce power ((a): run-of-river plant, (b)-(c) reservoir or pondage plants)). The indexing convention is also presented on the graph, with integers used for vertices and couples of integers for edges. $i + 1$ is the HTU directly downstream of i (natural flow) while $\{i - 1\}$ denotes the ensemble of HTU flowing into HTU i . Similarly $(i, i + 1)$ is the natural outflow edge from HTU i while $\{(i - 1, i)\}$ represent the ensemble of inflow edges into HTU i , including basin transfers.

vertex	$V_{tot,i}$	Total maximum storage capacity of the reservoir located in HTU i (m^3)
	$V_{elec,i}, V_{recre,i}, V_{irri,i}$	Maximum storage capacity dedicated to respective water uses (hydropower, recreation and irrigation) of the reservoir located in HTU i (m^3)
	$H_{dam,i}$	Height of the dam located in HTU i (m)
	$V_i(t)$	Current total volume in the reservoir located in HTU i (m^3)
	$V_{min,i}(t)$	Minimal water volume in the reservoir, it evolves with time to account for recreation uses (see Fig. 5) (m^3)
	$h_{res,i}(t)$	Water level in the reservoir (m)
	$A_{res,i}(t)$	Surface of the reservoir (m^2)
edge	$P_{(i,j)}$	Installed hydropower capacity of the plant located on the edge (MW)
	$P'_{(i,j)}$	Installed pumping capacity of the plant located on the edge (MW)
	$H_{(i,j)}$	Nominal hydraulic head of the plant located on the edge, obtained with a full reservoir (m)
	$Typ_{(i,j)}$	Hydropower plant type (run-of-river, reservoir or PHS)
	$\eta_{(i,j)}$	Production efficiency of the plant (conversion of potential energy to power)
	$\eta'_{(i,j)}$	Pumping efficiency of the plant (conversion of power to potential energy)
	$E_{(i,j)}(t)$	Production of the plant on the edge (MWh)
	$E'_{(i,j)}(t)$	Power consumption (MWh) of the plant on the edge associated to water pumping

Table 1. Model attributes and variables describing reservoirs and hydropower. Prognostic variables are distinguished in bold

2.2 Dams and reservoir parametrization

In the initial version of ORCHIDEE (Polcher et al., 2023), each HTU i contains three natural water stores, characterized by their time constants (slow aquifer, fast aquifer, and stream storage). To represent water management we add a fourth store to the HTUs in which dams have been located to represent water storage in the reservoir (Fig. 3). This section presents the continuity equation for the water volume in this reservoir.

2.2.1 Prognostic equations for water stores

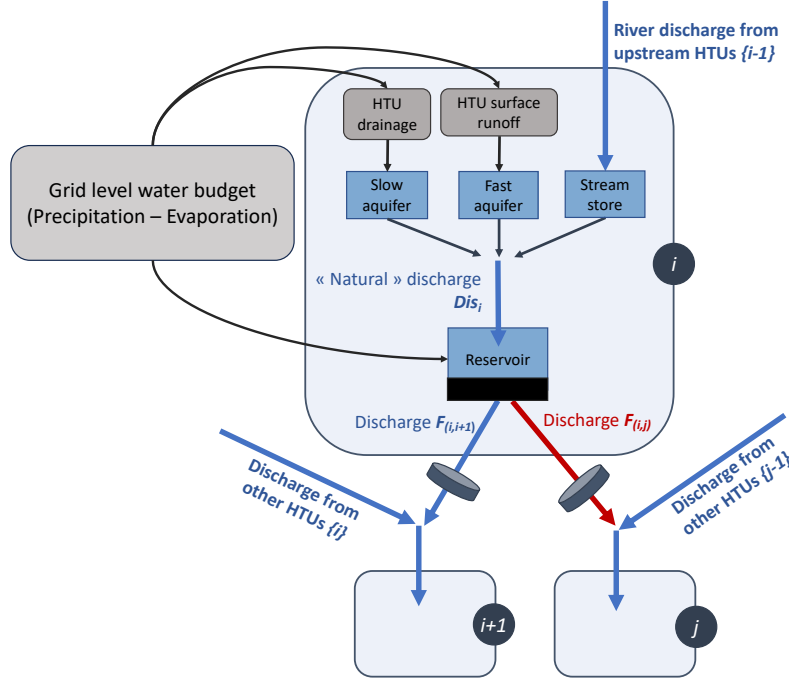


Figure 3. Schematic representation of water stores and flows in an HTU i

As represented in Fig. 3, the fast aquifer is filled by local runoff generated in the HTU, the slow aquifer by local drainage generated in the HTU, and the stream store by the discharge from upstream HTUs. The equations of these natural water stores are detailed in previous publications (Zhou et al., 2021; Polcher et al., 2023). They introduce the respective time constants of the natural stores g_{stream} , g_{fast} and g_{slow} (in unit $h.m^{-1}$) and the topographic index calculated for each HTU τ_i (in unit m^2).

The "natural discharge" $Dis_i(t)$ in the HTU i is generated by summing the outflows of the natural water stores (Eq. (1)). This natural discharge is stored in the reservoir if there is one in the HTU, or routed towards the downstream HTU if there is not.

$$Dis_i(t) = \frac{1}{\tau_i} * \left(\frac{W_{stream,i}(t)}{g_{stream}} + \frac{W_{fast,i}(t)}{g_{fast}} + \frac{W_{slow,i}(t)}{g_{slow}} \right) \quad (1)$$

The prognostic equation on reservoir volume is then given by:

$$\frac{dV_i}{dt}(t) = Dis_i(t) + p_{res,i}(t) - ev_{res,i}(t) - \underbrace{R_i \sum_j F_{(i,j)}(t)}_{\text{water release from the reservoir, which depends on the } F_{i,j}(t) \text{ is the water released from the HTU } i \text{ to the HTU } j, \text{ which breakdowns as:}} \quad (2)$$

215 where $p_{res,i}(t)$ and $ev_{res,i}(t)$ are respectively direct precipitation and evaporation over the reservoir, and $R_i(t)$ is the total water release from the reservoir, which depends on the $F_{i,j}(t)$ is the water released from the HTU i to the HTU j , which breakdowns as:

$$\underbrace{F_{(i,j)}(t)}_{\text{Reservoir releases aim at satisfying the different water demands addressed to the reservoir, in the limit of the available capacity. This release is computed based on:}} = \max \left(F_{(i,j)}^{ecol}(t), F_{(i,j)}^{irri}(t), F_{(i,j)}^{elec}(t) \right) + F_{(i,j)}^{spill}(t) \quad (3)$$

220 Reservoir releases aim at satisfying the different water demands addressed to the reservoir, in the limit of the available capacity. This release is computed based on: which are described in Sect. 2.3. Ecological and irrigation releases are limited by the demands addressed to the reservoir and the water available in the reservoir:

$$\underbrace{R_i F_{(i,j)}^{ecol}(t)}_{\text{demands addressed to the reservoir and the water available in the reservoir:}} = \max \min \left(\frac{V_i^*(t) - V_{min,i}(t)}{g_{res} * \tau_i}, \underbrace{Dw_i D_{(j,i)}^{ecol}(t)}_{\text{demands addressed to the reservoir and the water available in the reservoir:}}, \frac{V_i^*(t) - V_{tot,i}}{g_{res} * \tau_i} \frac{V_i^*(t) - V_{min,i}(t)}{\tau_{res}} \right) \quad (4)$$

$$\underbrace{F_{(i,j)}^{irri}(t)}_{\text{demands addressed to the reservoir and the water available in the reservoir:}} = \min \left(D_{(j,i)}^{irri}(t), \frac{V_i^*(t) - V_{min,i}(t)}{\tau_{res}} \right) \quad (5)$$

225 where $V_i^*(t)$ is the theoretical volume to be obtained without any release (Eq. (6)), $V_{min,i}(t)$ is the minimal volume and τ_{res} is the time constant of the reservoir, g_{res} is the time constant of the reservoir, and $Dw_i(t)$ is the total water demand addressed to the reservoir through its outflow edges which we assume to be of the order of magnitude of a few minutes.

$$\frac{dV_i^*}{dt}(t) = Dis_i(t) + p_{res,i}(t) - ev_{res,i}(t) \quad (6)$$

The water released for electricity generation is determined by the production of the plant, computed based on the distribution of the prescribed national demand (see Sect. 2.3).

$$230 \quad \underbrace{F_{(i,j)}^{elec}(t)}_{\text{demands addressed to the reservoir and the water available in the reservoir:}} = \frac{E_{(i,j)}(t)}{\rho g \eta_{(i,j)} h_{(i,j)}(t)} \quad (7)$$

where ρ is the water density, g is the gravitational constant, $\eta_{(i,j)}$ is the efficiency of the plant (set at 0.9 by default), and $h_{(i,j)}(t)$ is the current hydraulic head, which varies with the water level of the reservoir (Eq. (??), the different water demands are defined in Sect. 2.3)-8)).

$$\underbrace{h_{(i,j)}(t)}_{\text{demands addressed to the reservoir and the water available in the reservoir:}} = H_{(i,j)} - (H_{dam,i} - H_{res,i}(t)) \quad (8)$$

235 Finally, the spillage is defined as the water overflowing without being used for the different uses.

$$F_{(i,j)}^{spill}(t) = \begin{cases} \max\left(\frac{V_i^*(t) - V_{tot,i}}{\tau_{res}} - \sum_k \max\left(F_{(i,k)}^{ecol}(t), F_{(i,k)}^{irri}(t), F_{(i,k)}^{elec}(t)\right), 0\right) & , \text{if } j = i + 1 \\ 0 & , \text{else} \end{cases} \quad (9)$$

$$\frac{dV_i^*}{dt}(t) = Dis_i(t) + p_{res,i}(t) - ev_{res,i}(t)$$

$$Dw_i(t) = \max\left(D_{ecol.,(i+1,i)}(t), D_{irri.,(i+1,i)}(t), D_{elec.,(i+1,i)}(t)\right) + \sum_{j \neq i+1} D_{elec.,(j,i)}(t)$$

240 Reservoir release $R_i(t)$ generates water flows on the different edges connected to the HTU: $R_i(t) = \sum_j F_{(i,j)}(t)$, where:

$$F_{(i,i+1)}(t) = \min\left(R_i(t), \max\left(D_{ecol.,(i+1,i)}(t), D_{irri.,(i+1,i)}(t), D_{elec.,(i+1,i)}(t)\right)\right) + \max\left(R_i(t) - Dw_i(t), 0\right)$$

$$F_{(i,j)}(t) = \min\left(R_i(t) - F_{(i,i+1)}(t), D_{elec.,(j,i)}(t)\right), \text{ for } j \neq i + 1$$

245 The water flow to the river $F_{(i,i+1)}(t)$ is Ecological and irrigation flows $F_{(i,j)}^{ecol}(t)$ and $F_{(i,j)}^{irri}(t)$ are computed before the other flows $F_{(i,j)}(t)$, so we give priority to demands from the river downstream over any demand from power plants not located directly downstream of the reservoir. This is consistent, consistently with water management policy in most of the countries, where ecological demand takes priority over other non-vital water uses.

2.2.2 Diagnostic variables

Reservoir water level and surface

250 As in previous studies (Fekete et al., 2010; Zhou et al., 2018), we represent each reservoir i in the form of a tetrahedron of height $H_{dam,i}$ and volume $V_{tot,i}$ (Fig. 4).

We checked the validity of this assumption based on data available in the infrastructures dataset (see Appendix B). The height H of a tetrahedron, the area of the opposite face A and the volume V are linked by the relationship $H \times A = 3V$. By regressing $H_{res,i} \times A_{res,i}$ against $V_{res,i}$, we find a slope of 3.28 with a coefficient correlation of 0.93, which validates the geometry hypothesis.

255 Hence, the relations between the volume $V_i(t)$, the water level $H_{res,i}(t)$ and the area of the reservoir $A_{res,i}(t)$ are given by:

$$H_{res,i}(t) = H_{dam,i} * \left(\frac{V_i(t)}{V_{tot,i}}\right)^{\frac{1}{3}}$$

$$H_{res,i}(t) = H_{dam,i} * \left(\frac{V_i(t)}{V_{tot,i}}\right)^{\frac{1}{3}} \quad (10)$$

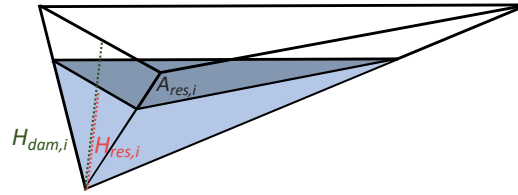


Figure 4. Geometry of the reservoir

$$\underline{A_{res,i}(t) = \frac{3 * V_i(t)}{H_{res,i}(t)}} \quad (11)$$

260

$$\underline{A_{res,i}(t) = \frac{3 * V_i(t)}{H_{res,i}(t)}}$$

Direct precipitation and evaporation (m^3/s) over the reservoir are then given by $p_{res,i}(t) = P_i(t) * A_{res,i}(t)$ and $ev_{res,i}(t) = Ev_i(t) * A_{res,i}(t)$ where $P_i(t)$ and $Ev_i(t)$ are respectively the precipitation and evaporation over the HTU i (in m/s). -

Hydropower production and pumping

265 The production $E_{(i,j)}(t)$ of an hydropower plant located on the edge (i,j) is:-

$$\underline{E_{(i,j)}(t) = \min\left(\rho g \eta_{(i,j)} h_{(i,j)}(t) F_{(i,j)}(t), P_{(i,j)}\right)}$$

where ρ is the water density, g is the gravitational constant, $\eta_{(i,j)}$ is the efficiency of the plant (set at 0.9 by default), $h_{(i,j)}(t)$ is the current hydraulic head (which varies with the water level of the reservoir (Eq. (8))) and $P_{(i,j)}$ is the installed capacity of the power plant.-

270 $\underline{h_{(i,j)}(t) = H_{(i,j)} - (H_{dam,i} - H_{res,i}(t))}$

Similarly, the power $E'_{(i,j)}(t)$ consumed by an hydropower plant located on the edge (i,j) to pump $F_{(j,i)}(t)$ is:-

$$\underline{E'_{(i,j)}(t) = \min\left(\frac{\rho g h_{(i,j)}(t) F_{(j,i)}(t)}{\eta'_{(i,j)}}, P'_{(i,j)}\right)}$$

275 where $\eta'_{(i,j)}$ is the pumping efficiency of the plant (set at 0.85 by default, following literature such as Wessel et al. (2020) and available data of French PHS production and pumping (RTE, b)) and $P'_{(i,j)}$ is the installed pumping capacity of the power plant.-

2.3 Water demands

Reservoirs ~~store water to fulfill several types of demand, such as domestic and industrial uses~~ are designed to store water for a variety of purposes, including energy production, irrigation, ~~energy production (hydropower and thermal plants) or~~

280 ~~tourism~~tourism, and domestic and industrial uses. As this study focuses on ~~hydropower~~hydroelectric reservoirs, we adopt a simplistic representation of the other water uses and only ~~detail water uses~~consider those that can constrain hydropower operations: ~~ecological flows, irrigation, and tourism~~.

~~In this subsection we describe the modeling approach we adopt to take into account some of these water demands.~~

2.3.1 Non-energy demands

285 2.3.2 **Ecological demand**

In many countries, the environmental laws require a minimum flow ~~$F_{min.,(i,i+1)}$~~ $F_{min.(i,i+1)}$ in the watercourse downstream of a dam in i , to guarantee the ecological quality of the river. ~~Minimal~~These minimal flow requirements depend on the region. Details for the French study case are presented in Sect. ~~3.3.1.~~

3.3.1. Such an ecological demand ~~$D_{ecol.,(j,i)}(t)$~~ $D_{(j,i)}^{ecol}(t)$ applies to all reservoirs regardless of their intended use:

$$290 \quad D_{ecol.,(j,i)}^{ecol}(t) = \begin{cases} F_{min.,(i,i+1)}, & \text{if } j = i + 1 \\ 0, & \text{else} \end{cases} \quad (12)$$

2.3.2 **Irrigative demand**

~~Some reservoirs also~~Some reservoirs store water for agriculture. Water withdrawals for irrigation can be made either directly from the reservoir or from the downstream river. Withdrawals from the river require a corresponding release from upstream reservoirs to maintain low flows. ~~In this study, the water requirements for irrigation are represented in a highly simplified manner by assuming a need proportional to $F_{min.,(i,i+1)}$ during the summer period. $D_{irri.,(i+1,i)}$~~ $D_{(j,i)}^{irri}(t)$ is then expressed in Eq. (13). The choice of the proportional factor α_{irri} and the delimitation of the summer period ~~are discussed~~may vary across regions. Details for our French case study are presented in Sect. ~~3.3.2.~~3.3.1.

$$D_{irri.,(j,i)}^{irri}(t) = \begin{cases} \alpha_{irri} * F_{min.,(i,i+1)}, & \text{if } j = i + 1 \text{ and } V_{irri,i} > 0 \text{ and } t \in Summer \\ 0, & \text{else} \end{cases} \quad (13)$$

2.3.2 **Tourism**

300 ~~In summer~~Finally, during the summer months, some reservoirs may also become ~~touristic areas~~tourist attractions where recreational activities are carried out and require the reservoir to be kept at a high level. To ensure proper reservoir filling during the summer season, dam operators follow a filling guide curve. We define corresponding constraints on $V_{min,i}(t)$ based on previous work and data available for French reservoirs (e.g. François (2013) on the Serre Ponçon reservoir), ~~see as shown~~Fig. 5.

305 By default, the minimum volume is set at 10% of the total capacity of the reservoir and is increased to 90% during the ~~touristic period for~~tourist season for the reservoirs concerned.

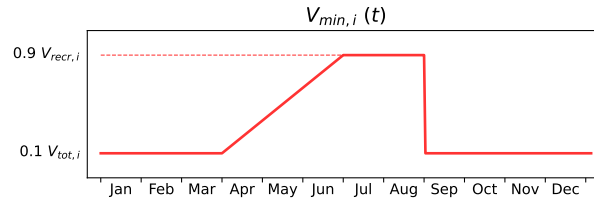


Figure 5. Evolution of the minimum volume constraints during the year

2.3.2 Hydroelectric demand

Production of hydropower plants is the result of the dispatch of the total power demand among the different power plants on the power grid (Stoft, 2002; Wood et al., 2013). Power generation units are called upon from least to most expensive to meet power demand at a minimal total minimal cost. Run-of-river power plants, whose production is free and non-dispatchable, are called upon first, along with solar and wind power plants, to produce to their maximum potential (as long as it does not exceed total demand, otherwise there is a curtailment of their production). On the contrary, the call upon reservoir and PHS dispatchable power plants is the result of a much more complex trade-off, aiming to minimize the total power system cost. From the point of view of a social planner, in charge of dispatch decisions and aware of the potentials and costs of all the units available in the network area, as well as the electricity demand, it is thus possible to define at each time step a demand for reservoir dispatchable hydroelectric power generation $D_{res}(t)$, PHS generation $D_{phs}(t)$ and PHS pumping $D'_{phs}(t)$ at each time step. These demands. This demand (or production targets) are target is defined for the whole grid and need needs then to be distributed among the different plant units plants to decide the amount of energy generated $E_{(i,j)}(t)$ (and consumed $E'_{(i,j)}(t)$) at each plant location, that will then drive reservoir release decisions. Indeed, knowing $E_{(i,j)}(t)$, the model deduces the hydroelectric water demand $D_{elec.,(j,i)}(t)$ as the additional water release needed for the plant production (Eq. (7)) and can finally compute the reservoir release based on Eq. (?) and (3).

$$D_{elec.,(j,i)}(t) = \max \left(\frac{E_{(i,j)}(t)}{\rho g \eta_{(i,j)} h_{(i,j)}(t)} - \max (D_{ecol.,(j,i)}(t) , D_{irri.,(j,i)}(t)) , 0 \right) + \frac{E'_{(j,i)}(t) \eta'_{(j,i)}}{\rho g h_{(j,i)}(t)}$$

To distribute national demand into individual plants production $E_{(i,j)}(t)$ (or consumption for pumping $E'_{(i,j)}(t)$), the model proceeds in two steps.

325 1) Fatal production and pumping:

The model starts by going through all the hydropower plants and calculates the energy they can produce or store without additional release, thanks to spillage (water that overflows) and other releases (ecological or irrigative irrigation) or the water expected to overflow. Associated production $E_{fatal,(i,j)}(t)$ and energy consumption $E'_{fatal,(i,j)}(t)$ $E_{spill,(i,i)}(t)$ are computed based on Eq. (?)14 and (?).

$$\begin{aligned}
330 \quad E_{fatal,(i,j)}(t) = & \min \left[P_{(i,j)} * \frac{h_{(i,j)}(t)}{H_{(i,j)}}, \right. \\
& \left. \frac{\min \left(\frac{V_i^*(t) - V_{tot,i}}{g_{res} \tau_i} - \max (D_{ecol.,(i+1,i)}(t) , D_{irri.,(i+1,i)}(t)), 0 \right) +}{\min \left(\max (D_{ecol.,(j,i)}(t) , D_{irri.,(j,i)}(t)), \frac{V_i^*(t) - V_{i,min}(t)}{g_{res} \tau_i} \right)} \right] \times \rho g \eta_{(i,j)} h_{(i,j)}(t)
\end{aligned}$$

15).

$$E_{fatal,(i,j)}(t) = \min \left(P_{(i,j)} \frac{h_{(i,j)}(t)}{H_{(i,j)}}, \max (F_{ecol,(i,j)}(t), F_{irri,(i,j)}(t)) \times \rho g \eta_{(i,j)} h_{(i,j)}(t) \right) \quad (14)$$

$$\begin{aligned}
335 \quad E'_{fatal,(i,j)spill,(i,j)}(t) = & \min \left(P'_{(i,j)} \frac{h_{(i,j)}(t)}{H_{(i,j)}} - E_{fatal,(i,j)}(t), \min \right. \\
& \left. \max \left(\frac{V_j^*(t) - V_{tot,j}}{g_{res} \tau_i} \frac{V_i^*(t) - V_{tot,i}}{\tau_{res}} - \max \left(\frac{D_{ecol.,(j+1,j)} F_{ecol,(i,i+1)}(t)}{\tau_{res}}, \frac{D_{irri.,(j+1,j)} F_{irri,(i,i+1)}(t)}{\tau_{res}} \right) \right) \right)
\end{aligned} \quad (15)$$

The remaining production demand to dispatch is then $D_k(t) - \sum_{Typ(i,j)=k} E_{fatal,(i,j)}(t)$ for k in {res,phs,pump}. $D_{res}(t) - \sum_{Typ(i,j)}$

340 **2) Reservoirs withdrawals:** If there is any national production (or pumping) demand left to dispatch ($D_{res}(t) > 0$), it should be produced by withdrawing water from the reservoirs. In this study, we consider that the reservoirs are used in the decreasing order of their relative filling to produce power, while respecting production constraints (installed capacity of the plant and the remaining volume of water in the reservoir). The remaining production is dispatched following this rule, until either all remaining production demand has been satisfied, or no more plants can produce. This rule leads to the equalization of relative

345 filling at the end of the each time step. This is equivalent to implementing a uniform rule curve for all reservoirs, as has been done in Dang et al. (2020). Another advantage offered by of this rule is that it leads to a production spread out over the whole territory. All plants are required to produce a little power each day, close to the so-called stable productions modeled in other studies (Sterl et al., 2020).

2.4 Validation diagnostics

350 The performance of our model to estimate hydropower production will be assessed based on three main diagnostics: the annual hydropower potential (AHP) simulated at each individual plant, the hydraulic stock simulated at the national level, and the time series of simulated production by hydropower plant type.

2.4.1 Hydraulic stock

355 Hydraulic stock notion refers to the total energy that can be produced using energy stored in all the reservoirs of the power grid, it is defined by (Eq. (17)).-

$$S(t) = \sum_{(i,j) \text{ s.a. } Typ_{(i,j)} = \text{reservoir}} \int_{V_{min,i}(t)}^{V_i(t)} \rho g \eta_{(i,j)} h_{(i,j)}(V) dV$$

2.4.1 Time-series of simulated production by hydropower plant type

For a hydropower plant type k , the simulated production $E_k(t)$ is given by $E_k(t) = \sum_{(i,j) \text{ s.a. } Typ_{(i,j)} = k} E_{(i,j)}(t)$ (where $E_{(i,j)}(t)$ is defined in Eq. (??) and k belongs to {run-of-river, reservoir, phs}).-

360 2.4.1 Annual hydropower potential (AHP) of an individual plant

For run-of-river and reservoir plants, we We define $AHP_{(i,j)}(y)$ as the maximum energy which that could be produced by the plant (i,j) over the year y in our simulation. -To compute it, we run a simulation in which the hydroelectric demand demand for dispatchable hydropower $D_{res,t}$ is fixed to infinite, leading all hydroelectric reservoir-reservoirs to release water within the limits of water availability and the installed capacity of the plant. Simulated-The simulated water flow $F_{i,j}(t)$ at the plant
365 location is then used to compute $AHP_{(i,j)}(y)$ based on Eq. (??16), considering the average head of each plant $\overline{h_{(i,j)}}$:-

$$AHP_{(i,j)}(y) = \int_{t \text{ in } y} \min\left(\rho g \eta_{(i,j)} \overline{h_{(i,j)}} F_{(i,j)}(t), P_{(i,j)}\right) dt$$

The average head $\overline{h_{(i,j)}}$, which is determined based on Eq. (8), taking the average reservoir water level. Observations of the average hydraulic stock combined with an assumption of identical average filling for every reservoir allows to compute the average filling with-

$$370 \quad AHP_{(i,j)}(y) = \int_{t \text{ in } y} \min\left(\rho g \eta_{(i,j)} \overline{h_{(i,j)}} F_{(i,j)}(t), P_{(i,j)}\right) dt \quad (16)$$

The hydraulic stock is the total energy that can be produced using energy stored in all the reservoirs of reservoir plants belonging to the power grid, it is defined by (Eq. (17)). This leads to an average filling of 63%. Then, Eq. (8) leads to $\overline{h_{(i,j)}} = H_{(i,j)} - 0.14 * H_{dam,i}$.

$$S(t) = \sum_{(i,j) \text{ s.a. } Typ_{(i,j)} = \text{reservoir}} \int_{V_{min,i}(t)}^{V_i(t)} \rho g \eta_{(i,j)} h_{(i,j)}(V) dV \quad (17)$$

375 Finally, for a hydropower plant type k (run-of-river or reservoir), the simulated production $E_k(t)$ is given by:

$$E_k(t) = \sum_{(i,j) \text{ s.a. } Typ_{(i,j)} = k} E_{(i,j)}(t). \quad (18)$$

2.5 Calibration

380 A calibration step is performed based on the comparison of simulated AHP and observed production at each individual plant, provided that such data is available. The objective of this step is to identify and correct errors from different sources, which are discussed in this section. The calibration procedure then varies according to the type of power plant.

2.5.1 Run-of-river plants

A discrepancy between the simulated AHP of a run-of-river plant and its historical production can be attributed to five factors:

1. A hydro-meteorological bias may result in discrepancies in river discharges between the model and the actual river conditions;
- 385 2. An inexact location of the hydropower plants during the placement on the HTU graph may lead to inaccurate estimations of the available discharge at the plant location;
3. We assume that the plant can harness the entire river volume. In reality, the river can be divided into several branches, with only one of them passing through the plant;
- 390 4. Plants efficiencies are assumed to be equal for all plants and constant to 0.9. In reality, the efficiency of a hydropower plant depends on the type of hydroelectric turbine that is used (the choice is made based on the plant's rated head and flow) and varies with the flow rate;
- 395 5. We assume that plants produce at their maximum potential. However, in reality, a plant may be unavailable for a period of time due to maintenance. Moreover, some of the plant's potential can be reserved for ancillary services to the grid or curtailed if the non-dispatchable potential production of renewables exceeds the power demand. This can reduce the actual production compared to the potential.

As in previous studies (Wagner et al., 2017; Zhou et al., 2018), the unknown efficiency of the power plant $\eta_{(i,j)}$ is adjusted to calibrate the model to the historical annual generation data based on previously estimated bias (Eq. (19)). Such calibration corrects the total error without differentiating its source.

$$\eta_{(i,j)} = \frac{1}{0.9} * \frac{E_{(i,j)}(y)}{AHP_{(i,j)}(y)} \quad (19)$$

400 2.5.2 Poundage and reservoir power plants

Over a year, all the water entering the reservoir i of a plant (i, j) could either contribute to the annual production of the plant $E_{(i,j)}(y)$, to the annual change of the hydraulic stock in the reservoir $\Delta S_i(y)$ or spill without generating power.

As for run-of-river plants, differences in simulated AHP and observed production can have different sources. In addition to the five errors listed above, a sixth possible error, related to the adduction network, should also be considered. Indeed, we

405 assume in our model that each plant is only fed by one reservoir, which can lead to an underestimation of the plant production if some other water inputs are non-negligible. To account for these different error sources, we calibrate the model in two successive steps:

- Step 1: Dams with a large negative bias (inferior to -50 %) are shifted downstream from their original location to take into account the computed deviation. This can be interpreted as the addition of water inlets for the power plant based on the topography such that the power plant receives enough water. Most concerned areas are located in mountains, where the water intakes are quite close geographically (on the same atmospheric grid) and therefore subject to the same precipitation, which allows us to assume that the water available per unit of area is similar.
- Step 2: Once the network error is corrected, the efficiencies of the plants are adjusted to match the observed production, as with run-of-river (Eq. (19)).

415 3 Data and methods for the test case over France

~~To validate this modeling approach, the proposed method is applied to the French power grid.~~

3.1 ORCHIDEE setup

In this study, ORCHIDEE is run in stand-alone mode, forced with the SAFRAN meteorological data set (Quintana-Segui et al., 2008). SAFRAN (Système d'Analyse Fournissant des Renseignements Atmosphériques à la Neige) is a surface reanalysis
420 resulting from the optimal interpolation between the vertical profiles of the atmosphere derived from ERA-40 atmospheric reanalysis and surface observations. It provides the required atmospheric variables - temperature, relative humidity at two meters, wind speed, downward radiation (shortwaves and longwaves), and precipitation (solid and liquid) - at an hourly time step over an 8×8 km grid that covers France and upstream part of ~~the international~~ its catchments beyond its borders.

To estimate the sensitivity of ORCHIDEE's simulations to the uncertainties of precipitation, we built two alternative atmospheric forcings by replacing precipitation data in SAFRAN with other precipitation datasets: COMEPHORE (Tabary et al.,
425 2012) and SPAZM (Gottardi et al., 2008). These datasets are presented in detail in Appendix C1 and their relative differences with SAFRAN are displayed in Fig. C1.

COMEPHORE dataset provides observations of surface precipitation accumulation over metropolitan France at an hourly and kilometric resolution based on a synthesis of radar and rain gauge data. We build a meteorologic dataset SAF_COM by
430 replacing precipitation data in SAFRAN with data from COMEPHORE. As COMEPHORE does not distinguish solid and liquid precipitations, we keep SAFRAN's hourly ratio of solid/liquid precipitations when possible and discriminate based on the air temperature otherwise. The differences in annual mean precipitation between SAFRAN and COMEPHORE are generally small, with an average deviation inferior to 1.0% in COMEPHORE compared to SAFRAN (Fig. C1). However, we find a small seasonal bias as this average deviation goes from -2.0% for the Winter period to +1.9% in the Summer. Moreover,

435 discrepancies increase dramatically in mountainous regions, especially in the Alps and in the Pyrenees. For grid points with an average elevation above 1000m, the annual mean precipitation in COMEPHORE is, on average, 10.4% lower.

SPAQM is a daily reanalysis of precipitation at the ~~kilometer-scale~~kilometer scale, developed by EDF, the main electricity producer in France. We interpolate the daily precipitation data from SPAQM to the hourly scale and merge it with SAFRAN data to create the alternative forcing dataset SAF_SPAQM. As for SAF_COM, we keep SAFRAN's hourly ratio of solid/liquid
440 precipitations when possible. Compared to SAFRAN, precipitations are ~~in-on~~on average 2.7% higher in SPAQM with an average bias of 7.0% in Summer, against 2.1% in Winter. Bias is heterogeneously spread over France (Fig. C1) with bigger differences on the highest reliefs, without a clear sign (average deviation of +3.9% for grid points above 1000m).

Appendix E provides an extensive assessment and discussion of hydro-meteorological biases in ORCHIDEE simulations over French rivers. In particular, we identified uncertainties in observed precipitation as a main contributor to the error in
445 simulated discharge, especially in the mountains.

The vegetation distribution map used in ORCHIDEE is derived from the ESA-CCI Land Cover dataset at 0.05° resolution for the year 2010. The soil background albedo map is derived from the MODIS albedo dataset aggregated at 0.5° resolution. Soil texture distribution maps are obtained from Reynolds map (Reynolds et al., 2000) at 5-arc-min resolution with 12 USDA soil texture classes (at 30 cm depth).

450 ~~In our~~In this study, ORCHIDEE performs the energy and water budgets at a 15-minute time step and hydropower operations are performed at the same time step. Given that the time step is greater than the time constant of reservoirs, we consider that reservoir spillage always occurs within a single time step.

3.2 ~~Locating hydroelectric infrastructures on the routing network~~

~~As explained in Sect. 2.1, the first step in building the routing network is to locate the infrastructures on the high-resolution~~
455 ~~river network based on the information provided in infrastructures datasets. The infrastructures datasets we use in this study~~

3.2 Hydroelectric infrastructure

The infrastructure datasets are presented in detail in Appendix B. We ~~assess here the quality of this location~~use reservoir data
460 from GRanD (Global Reservoirs and Dams) (Lehner et al., 2011) and CFBR (CFBR, 2021) datasets. Data provided in these datasets allow us to validate the assumption about reservoir geometry (Fig. 4). For hydropower plants, we use data from the
EU Joint Research Center hydropower plants database (European Commission and Joint Research Centre (JRC), 2019) and national registers of electricity generation and storage facilities published annually by the French TSO (ODRÉ, 2016, 2018).

Following the procedure outlined in Fig. 1, we locate the infrastructures on the MERIT river network and construct the HTUs routing graph based on the simplification of this MERIT network (resolution of 2km) on the SAFRAN atmospheric grid (resolution of 8 km). HTUs area can thus theoretically vary from 0 to 64 km^2 and the average area of HTUs in our graph is
465 4.73 km^2 .

The upstream area of an HTU is defined recursively as the sum of the HTU area and the upstream area of all its tributaries. For each hydroelectric infrastructure, we compare in Fig. 6 its reference upstream area (from the database or MERIT network)

to the upstream area of the HTU in which it is located. For most of the structures, the positioning error is lower than 20%. Some dams with a small upstream area are, however, located in HTUs with a higher upstream area, due to resolution constraints.

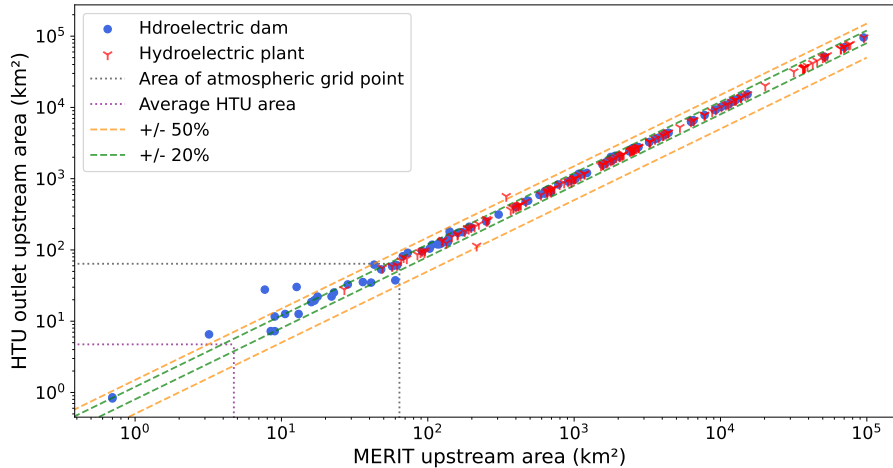


Figure 6. Comparison of the initial upstream area of the infrastructure (referenced in the database or upstream area of the MERIT pixel on which it is placed) with its final upstream area in the HTUs graph. Blue dots represent hydroelectric reservoirs (reservoirs that have been associated with power plants during the adduction network building step) and red signs represent hydropower plants. Green and orange dashed lines delineate a respective error of +/- 20% and +/- 50% while grey and purple dotted lines refer to the respective atmospheric grid point area and average area of an HTU.

470 3.3 Data for water demands and validation

3.3.1 Ecological and irrigation demands

In France, minimal flow requirements are defined relatively to the mean interannual flow upstream of the dam \overline{Dis}_i (Code de l'Environnement, Article L214-18). They are summarized in Table 2. We ran a twenty-year SAFRAN simulation without reservoir operations to calculate \overline{Dis}_i at dam locations.

	$\overline{Dis}_i > 80m^3/s$	$\overline{Dis}_i < 80m^3/s$
Dam intended for hydropower purpose	$F_{min,(i,i+1)}(t) = 5\% * \overline{Dis}_i$ or flow immediately upstream of the dam if it is lower	$F_{min,(i,i+1)}(t) = 5\% * \overline{Dis}_i$ or flow immediately upstream of the dam if it is lower
Dam intended for other purpose	$F_{min,(i,i+1)}(t) = 5\% * \overline{Dis}_i$ or flow immediately upstream of the dam if it is lower	$F_{min,(i,i+1)}(t) = 10\% * \overline{Dis}_i$ or flow immediately upstream of the dam if it is lower

Table 2. French legal requirements for ecological flow, \overline{Dis}_i is the mean interannual flow downstream of the dam

475 To account for the irrigation purposes of some reservoirs, we increase the minimal flow requirement downstream of reservoirs intended for irrigation during the summer period (June 1st to September 30th) by setting $\alpha_{irri} = 8$. This choice is based on information available from French reservoir concession contracts, which sometimes specify the volume of water reserved for irrigation. In the case of Serre-Ponçon, for example, the concession contract stipulates a reserve of 200 million m^3 , to be used for irrigation, between July 1 and September 30. If we consider a constant withdrawal spanning three months, this corresponds
480 to a $25m^3/s$ flow, which is 45% of the $55m^3/s$ mean interannual flow at this location, and thus 9 times larger than F_{min} , which is set to 5%, as explained above.

3.3.2 Hydropower production demand

As this study aims to validate our proposed reservoir operations model, we take the ~~historie~~historical time series of production as the hydropower demand prescribed to the model. We can thus assess if the reservoir operations performed by the model
485 when it is forced by the historical atmospheric dataset can meet the observed production.

Data of observed production for hydropower plants in the French power grid are published from 2015 onwards by the French electricity transmission system operator RTE at a 30-minute ~~timestep for 4~~time step for 2 categories of plants (RTE, a):

- ~~Run-of-river~~ River production $D_{river,t}$ that gathers the production of pure run-of-river power plants and poundage power plants (reservoir plants with a ~~limited storage capacity called "poundage"~~ (distinction defined by French operators storage below 400h))
490
- **Reservoir production** $D_{res,t}$ that gathers the production of reservoir power plants with a greater storage capacity
- ~~PHS production that gathers~~

In our model, $D_{river,t}$ is then used to drive the production of PHS power plants PHS pumping that gathers the consumption of PHS power plants for pumping run-of-river and poundage power plants, while $D_{res,t}$ is used for the reservoir power plants with greater storage capacity, both using the method described in 2.3.2. We use the classification established by RTE and illustrated in Fig. B2.
495

3.3.3 Validation data

In France, hydroelectricity is produced by companies that do not share precise data on the production of their power plants or the filling of the reservoirs they manage. Similarly, discharge data from gauging stations near hydroelectric power plants are
500 often inaccessible to the public. This limits the available data for validating our model.

However, as a delegate of public services, RTE provides data, often aggregated at the national level, which allows us to calibrate and validate our model as shown in the following two sections.

The available data is:

- National ~~time-series~~time series of production by hydroelectric sector (river and reservoir) at 30-minute time step from
505 2015 (RTE, a) - which are the ~~time-series~~time series used for the hydropower production demand;

- Annual production of each hydroelectric power plant for the years 2015, 2016, and 2018 (ODRÉ, 2015, 2016, 2018);
- Weekly hydraulic stock (Eq. (17)) at national level from 2014 to 2020 (RTE, c);

As mentioned in Appendix B, our final hydropower plants dataset does not include all the hydropower plants installed in France. However, using annual production data of each plant provided by (ODRÉ, 2015, 2016, 2018), we can quantify the share of the national production provided by the power plants in our database. This enables us to compute a factor to convert the actual production of national ~~time-series~~ time series (RTE, a) into representative production in our model both for prescribing the production demand and comparing the results. The calculation of such conversion factors is presented in Table B2. ~~It relies on the assumption that within each category of power plant, the geographical distribution of plants in our database is representative of all French power plants so that production ratios remain constant over time. This assumption is debatable as our database includes the largest power plants in terms of installed capacity, which are predominantly concentrated in certain regions, while smaller scale plants may be located in watersheds not represented in our database (e.g., run-of-river plants on the River Seine for instance). However, as the missing plants have, by definition, a lower installed capacity than those in our database, their contribution to national production is lower and can reasonably be neglected.~~

We ~~compute the total energy storage capacity~~ also compute the maximal hydraulic stock of the reservoirs associated with the power plants in our database using Eq. (17) and data from our plants and reservoirs databases. We obtain $S_{max} = 3.66 TWh$, which is quite close to the 3.59 TWh value reported by RTE (RTE, c). Therefore, we can consider that our database covers all the available storage and that missing hydropower capacity is linked to negligible reservoirs.

3.4 **Hydro-meteorological errors**

4 Results

~~To evaluate the performance of the ORCHIDEE model to simulate river discharges in France, independent of reservoir operations, we compare daily river discharges simulated by the model with the observations database of Schapi (2022). It is important to acknowledge that the observed discharge data represents actual discharge values, including water withdrawals, while at this stage, our model generates natural discharges without such withdrawals and dam operations.~~

4.1 Calibration

530 4.1.1 **Bias in average discharge**

~~Figure E1 displays relative biases of average discharge simulated by ORCHIDEE forced by SAFRAN over the 2010-2020 period for a selection of gauging stations located on rivers equipped with hydropower infrastructure (see Fig. B2 for the detailed locations of the power plants). We chose the bias metric because the annual mean discharge is the most relevant parameter for hydropower potential.~~

535 ~~Relative bias of average discharge for a selection of gauging stations located on French rivers equipped for hydropower for the period 2010-2020. Each colored point represents a gauging station, The shape indicates the size of the concerned watershed~~

while the color indicates the calculated bias at this location. Purple stars indicate the locations of the hydropower plants located on the grid. Source: authors, based on a layer by U.S. National Park Service

The overall performance of the model indicates a slight overestimation of flows, with an average bias of +2.4%.

540 The discharge bias shows an increasing trend with the upstream area of stations. For small catchments (less than 500 km^2), the average bias is -1.6%. In medium-sized catchments (between 500 and 5000 km^2), the bias decreases to +1.1%. In large catchments (more than 5000 km^2), the bias becomes more pronounced, reaching 7.6%. It is however important to note that the smaller the upstream area, the greater the uncertainty in the location of the station. In Fig. E1, only the stations located with an error in the upstream area lower than 20% are displayed.

545 On the largest rivers (Rhine and Rhone), where most run-of-river power plants are located, the bias shows little spatial variability, constant at around +20% for the Rhone and -10% for the Rhine respectively. In the Alps, on the other hand, where a significant proportion of dispatchable hydroelectric capacity is installed, the bias displays a high spatial heterogeneity, sometimes within the same river. Upstream of the Isere river, the bias varies from -19% to +26% between two stations some twenty kilometers apart. The upstream reaches of the Durance also show negative biases.

550 In the other massifs equipped for hydroelectricity (the Pyrenees and Massif Central), there are also negative biases at altitude, which gradually diminish downstream.

Assuming negligible observational errors, discharge bias can originate from different error sources:-

- Errors in the atmospheric forcing applied to ORCHIDEE;
- Modeling errors in the energy, water, and carbon cycles;
- 555 - Missing processes in ORCHIDEE-like glacier melting, interactions with groundwater, and water withdrawals).

To explore the first hypothesis, Fig. E2 compares discharges simulated by ORCHIDEE using the two alternative forcings (SAF_COM and SAF_SPAZM) with the reference SAFRAN simulation. The relative biases of these simulations to observations are presented in Fig. E3.

560 Average relative bias in discharge simulated by ORCHIDEE under alternative precipitation forcings. Results are given in relative difference compared to the reference SAFRAN simulation, for the period 2010-2020. Left: annual average bias, middle: average bias in the Winter period (December-January-February), right: average in the Summer period (June-July-August). The discharges are displayed for all grid points with an upstream area higher than 1000 km^2 .

565 Relative bias of average discharge simulated by ORCHIDEE under alternative forcings for a selection of gauging stations located on French rivers equipped for hydropower for the period 2010-2020. The left coloring indicated the average bias of discharges simulated under SAF_COM while the right coloring indicated the average bias of simulations under SAF_SPAZM. Source: authors, based on a layer by U.S. National Park Service

Under SAF_COM, simulated discharges show relatively small differences on annual average, except in mountainous watersheds (Alps and Pyrenees), where the lower precipitation in COMEPHORE results in streamflows that are 30% to 40% lower when compared to the SAFRAN simulation. However, a pronounced seasonal pattern is observed. The simulated streamflows in

570 winter are lower in the simulation forced by COMEPHORE across France (averaging -16% and up to -50% for the Loire and
Durance rivers), while in summer, they are higher (averaging +25% and up to +50% for the Loire River). As regards comparison
with observed flows (Fig. E3, the negative biases existing under SAFRAN in the Alps and Pyrenees are accentuated, particularly
along the Durance and Isère rivers where many hydroelectric power plants are located. However, for some Alpine stations
and the Massif Central, for which the flow is overestimated with SAFRAN, the flow is more accurately simulated with
575 COMEPHORE.

Under the SAF_SPAZM forcing, river discharges show an increase in the majority of watersheds, which is consistent with
the previously highlighted higher precipitation in this dataset. However, the upper Rhone watershed stands out with a decrease
in simulated discharge, reaching up to -40% during the summer season, allowing for a reduction in the bias of simulated
discharges in this area.

580 Even if we limit our analysis to the precipitation variable without considering other forcing variables, we show a significant
influence of the forcing variability on the simulated discharges.

4.1.1 Discharge seasonality

Beyond the bias in average values, the performance of ORCHIDEE in reproducing the seasonality of the discharge is key for the
modeling of run-of-river production as well as that of poundage power plants, which have only a very limited storage capacity.
585 Observations and simulations of daily discharges under SAFRAN forcing are presented in Fig. E4 for selected gauging stations
in catchments equipped with run-of-river or poundage power plants.

As depicted in Fig. B2, run-of-river plants are mostly located along the Rhone and Rhine rivers. In the upper Rhone (Surjoux
station), there is a substantial overestimation of high flows and an underestimation of low flows. The error reduces progressively
downstream: the Nash Sutcliffe efficiency (NSE) is better at the Valence station, despite a higher overall annual bias (likely due
590 to the non-representation of water withdrawals). On the Rhine (Basel and Strasbourg stations), we see similar errors, with an
underestimation of low flows during the Fall and an underestimation of the Spring maximum. The discrepancy in the Rhone's
seasonality can be attributed to the non-representation of Lemman reservoir management in our model, which is known to play
a crucial role in shaping discharge seasonality in the upper Rhone (Habets et al., 1999).

Poundage plants are distributed across various catchments. Some of them are concentrated in the upper Dordogne river,
595 notably the Chastang plant, the most powerful poundage facility, which benefits from a gauging station at its location. We find
a positive NSE for this station, indicating that the seasonality is well captured by the model.

Finally, some run-of-river and poundage plants are also concentrated in the Alps, where we focus on two gauging stations:
Chamonix, situated in a small upper catchment, close to a run-of-river plant and Cheylas, positioned on a large river (l'Isère),
downstream from several power plants. At Chamonix, we find a seasonal bias as the model simulates an earlier discharge
600 peak compared to observations (around 2 months ahead). At Cheylas, the model overestimates the seasonal variability of the
discharge, with higher flows during Spring and lower flows during Winter, which can be attributed – at least in part – to the
non-representation of reservoir management at this stage of our study (see Sect. 4.2).

Comparison of simulated and observed river discharges for a selection of gauging stations. Locations of selected stations are indicated in Figure E1. Fines lines and dots are daily time series while ticker lines are 30-day sliding averages. NSE-metrics are computed on a daily time series.

5 Calibration of the hydropower operation model

The hydro-meteorological biases highlighted in the previous section can lead to significant errors in the estimation of hydroelectric production. However, the limited knowledge of actual hydropower networks (unknown values for plant efficiency, uncertainty of the water input of reservoir plants) can also contribute to similar errors.

In this section, we estimate the differences between AHPs (We present here the application of the calibration process to the French study case. We assess the discrepancy between the AHP simulated by the model (Eq. (16)) simulated by the model, and the observed annual production at each power plant (as mentioned earlier, this data is available for the years 2015, 2016, and 2018). We discuss the with available data. The likely origin of these differences and propose a calibration method for the unknown parameters to address these differences, to make the hydrological cycle simulated in ORCHIDEE consistent with observed production.

We first describe the calibration approach for run-of-river power plants, and then for reservoir power plants discrepancies is then discussed. Finally, we validate this calibration the calibration process is validated by comparing annual potentials simulated in ORCHIDEE to the observed annual production at the national level on for an extended period (data available from 2000 to 2020). We choose to use SAFRAN forcing as a reference for the calibration step, as this dataset is widely used in regional studies of France.

4.1 Run-of-river plants

As curtailment of run-of-river production is generally not assumed, AHPs (Eq. (16)) should therefore be a good approximation of the observed production. A bias in the simulated AHP of a run-of-river plant compared to its historic production can be explained by five reasons:

1. Hydro-meteorological bias leading to different river discharges in the model. These errors have been assessed in the previous section;
2. An inexact location of the hydropower plants during the placement on the HTU graph, which leads to over/underestimation of the available discharge at the plant location. However, Fig. 6 shows that the error is less than 10% for most of the plants we placed on the river network;
3. We assume that all the water of the river can be exploited by the plant. In reality, the river can be divided into several branches with only one of them passing through the plant;

4. ~~Plants efficiencies are assumed to be equal for all plants and constant to 0.9. In reality, the efficiency of a hydropower plant depends on the type of hydroelectric turbine that is used (the choice is made based on the plant's rated head and flow) and varies with the flow rate;~~
- 635 5. ~~We assume that plants produce at their maximum potential. However, in reality, a plant can be unavailable for some period—due to maintenance, for instance. Moreover, some of the plant's potential can be reserved for ancillary services to the grid. This can reduce the actual production compared to the potential.~~

4.0.1 Discrepancies between AHP and the historical production

Fig. Figure 7 shows the average relative bias in simulated AHP compared to observed production for the three years with available data for the run-of-river plants in our database. For most of the plants, the majority of plants, the bias in hydropower potential is close comparable to the bias in river discharge computed at neighboring stations displayed in Fig. E1, meaning indicating that it mainly comes from the hydro-meteorological error (reason 1 of the list presented in Sect.2.5). At Caderousse (on Rhone) and Gamsheim (on the Rhine), the Caderousse and Gamsheim power plants, located in Fig. 7, a stronger positive bias is found. At these locations, only part of the river passes through the plant (reason 2).

645 ~~Average relative bias (in %) of simulated annual hydropower potential compared to observed historic production for run-of-river plants with available data. Point size corresponds to average annual production. Source: authors, based on a layer by U.S. National Park Service~~

650 ~~As in previous studies (Wagner et al., 2017; Zhou et al., 2018), the unknown efficiency of the power plant $\eta_{(i,j)}$ is adjusted to calibrate the model to the historical annual generation data based on previously estimated bias (Eq. (19)). Such calibration corrects the total error without differentiating its source.~~

$$\eta_{(i,j)} = \frac{1}{0.9} * \frac{E_{(i,j)}(y)}{AHP_{(i,j)}(y)}$$

~~Obtained efficiencies range, which may contribute to the observed bias (reason 3). The calibration leads to obtained efficiencies ranging~~ from 0.43 to 1.31 with a median value of 0.88.

4.1 Reservoir plants

655 Over a year, all the water entering the reservoir of a reservoir or poundage power plant could either contribute to the annual production of the plant $E_{(i,j)}(y)$, to the annual change of the hydraulic stock in the reservoir $\Delta S_i(y)$ or spill without generating power. Observed production $E_{(i,j)}(y)$ is available for the three years mentioned earlier, however observations of the change of the hydraulic stock are only available at the national level for the national stock $\Delta S_{obs}(y) = \sum_{i \text{ in res}} \Delta S_i(y)$. To compare simulated AHPs with observations of production and stored energy, we make the two following assumptions: (i) spillages

660 that do not produce power can be neglected and (ii) the change in the hydraulic stock is homogeneous across all reservoirs:

$$\forall i, \Delta S_i(y) = \Delta S_{obs}(y) \times \frac{S_{max}}{S_{i,max}}$$

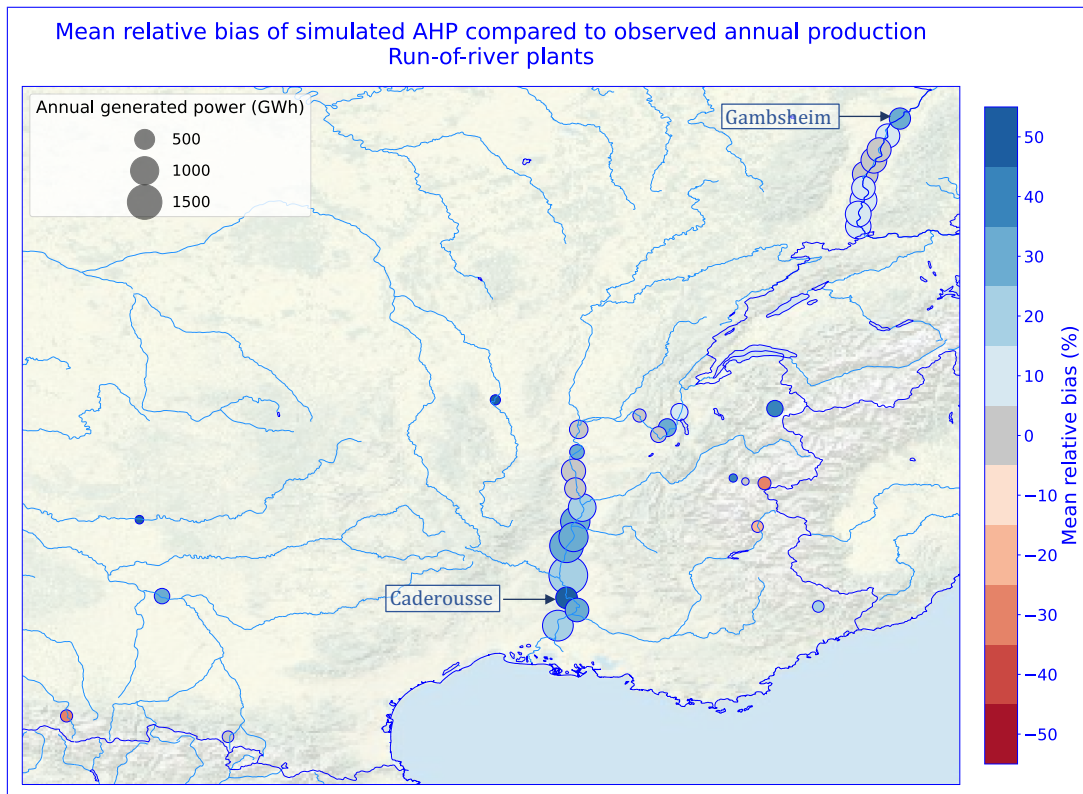


Figure 7. Average relative bias of simulated annual hydropower potential compared to observed historical production for run-of-river plants with available data. The point size corresponds to the average annual production.

Source: authors, based on a layer by U.S. National Park Service

In Fig. 8, we plot the average bias of $AHP_{(i,j)}(y)$ relative to observed net production $E_{(i,j)}(y) + \Delta S_i(y)$ for the three years for which data is available. It enables us to distinguish two types of bias in the simulated AHP, suggesting that two main error sources can be distinguished:

- 665 – Plants that have an absolute bias inferior to 50% (represented by circles in Fig. 8). Their biases are generally similar to the one of discharge for neighboring stations in Fig. E1.
- Plants that have a bias inferior to -50% (represented by pentagons in Fig. 8). These plants are mainly located in mountain areas and have a negative bias larger than the one of the discharges in this area. Moreover, their biases have a small interannual variance, indicating that the error is stable in time (not shown).

670 ~~As for run-of-river plants, differences in simulated AHP compared to observed production of reservoir plants can have different sources. In addition to the five errors listed above that apply also to reservoir plants, a sixth possible error, related to~~

Mean relative bias of simulated AHP compared to observed annual production Reservoir plants

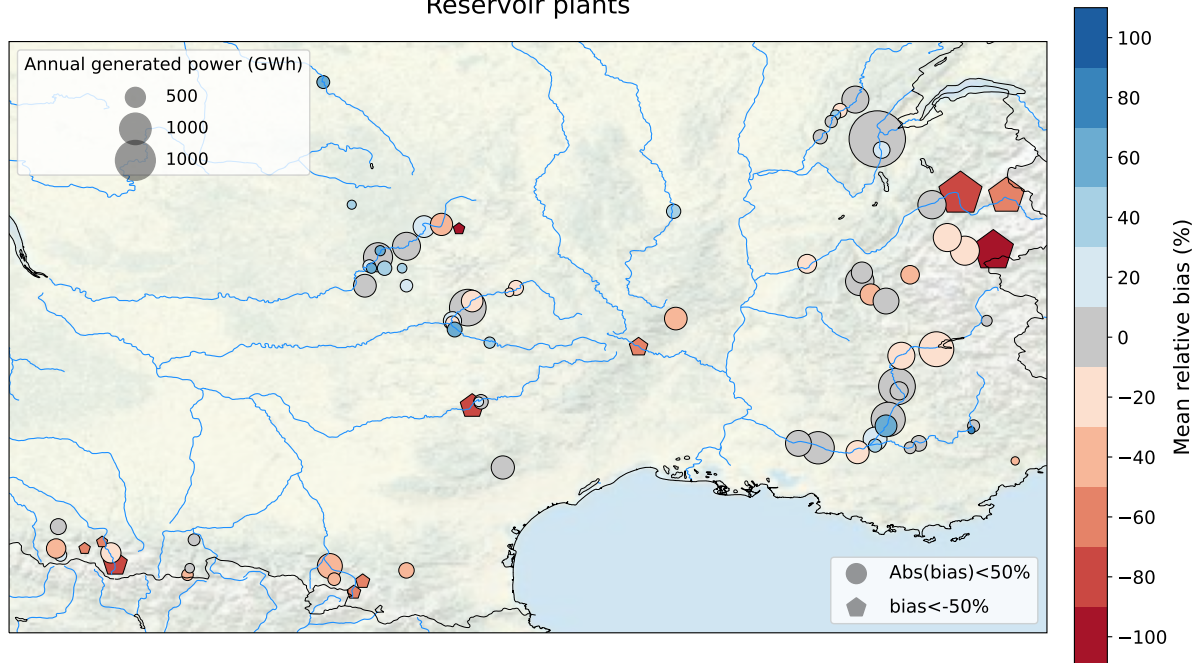


Figure 8. Average bias in [the](#) simulated AHP compared to [the](#) observed [historie](#)-[historical](#) net [annual](#) production of reservoir [and](#) [poundage](#) [power](#) plants [with available data](#). [Points](#)-[The point](#) size corresponds to the average annual production of the plant.

Source: authors, based on a layer by U.S. National Park Service

~~the~~ ~~adduction~~ ~~network~~, should also be considered. Indeed, we assume in our model that each plant is only fed by one reservoir, which can lead to an underestimation of the plant production if some other water inputs are non-negligible.

675 For the first category of plants, the first reason (hydro-meteorological error) can explain most of the computed bias. For the second category, however, the sixth reason (error on the adduction network) seems to be predominant. Indeed, mountain plants are fed by several water intakes, and thus the intake reservoir we are considering, even if it represents the main source of water, is only a small portion of the water input. Therefore, the simulated inflow at the reservoir location is not sufficient to generate the observed production, which can explain the large negative bias we find. The example of the La Bathie power plant in the Alps is detailed in Appendix D.

680 To account for these two different error sources, we calibrate the model in two successive steps:

- Step 1: Dams with a large negative bias (inferior to -50%) are shifted from their original location to take into account the computed deviation (they are located as if their upstream area was corrected by the ratio). This allows for the modeling of an entry point of the power plant which receives enough water. Most concerned areas are located in mountains, where the water intakes are quite close geographically (on the same atmospheric grid) and therefore subject to the same precipitation, which legitimizes this operation.

685

- ~~Step 2: Once the network error is corrected, the efficiencies of the plants are adjusted to match the observed production, as is with run-of-river. We find a median efficiency of 1.01.~~

4.1 ~~Validation of the calibration~~

4.0.1 Validation of the calibration

690 The performance of the calibrated model is assessed by comparing potentials simulated by the calibrated model forced by SAFRAN with the ~~historie~~-historical annual production (RTE, a) for the different categories of power plants over the whole period ~~(2010-2020) (Fig. 9)~~. We assume that hydropower is used as much as possible and that the production is well managed so that ~~actual production~~-the AHP is a good proxy to compare with ~~our potential production~~AHP. ~~To align with RTE's classification, we categorize the reservoir power plants into two groups: poundage and reservoirs.~~the actual production. For a
695 given category, the ~~annual simulated~~-simulated annual potential is computed by summing the ~~AHPs~~-AHP of all plants belonging to this category. For poundage and reservoir plants, we directly compare this aggregated potential to the ~~historie~~-historical production, as stock data (RTE, c) is not available for the whole period. This relies on the assumption that the national stock returns to its initial value at the end of each year.

The calibration appears to be robust as a very small bias (less than 3%) is obtained when comparing the simulated potentials
700 to the observed production ~~(Fig. 9)~~. The relative differences ~~of in~~ annual production are on average lower than 10%. This indicates that the model is able to capture the overall pattern of interannual variability of the observed production.

We also explore the sensitivity of our model and calibration procedure to the uncertainties in precipitation forcings highlighted in ~~Sect. E~~Fig. C1 and E2. We compute ~~annual hydropower potentials~~-AHPs under the two alternative forcings (Fig. 9)
and compare the inter-annual variability of observed production to the inter-forcing variability (Fig. 9)-

705 Tab. 3). Run-of-river annual potentials exhibit little variation across the different forcings, as the simulated flows of major rivers hosting run-of-river power plants (primarily the Rhone and the Rhine) demonstrate a low sensitivity to ~~atmospheric forcing~~-precipitation uncertainty (see Fig. E3). Consequently, the inter-forcing variability of simulated potential (defined as the mean standard deviation of annual potential across the forcings) is three times smaller than the interannual variability of run-of-river power production (defined as the standard deviation of observed annual productions), see Table 3. It is also slightly smaller
710 than the modeling error (RMSE of SAFRAN simulated potentials compared to observations), indicating a low sensitivity of simulated run-of-river production to the ~~atmospheric forcing~~-

precipitation uncertainty. Conversely, reservoir plant production shows a much higher sensitivity to precipitation disparities between forcings. Lower COMEPHORE precipitations in mountainous regions lead to an average decrease of 18.7% in the total simulated potential, compared to the SAFRAN simulation. As a result, the variability among forcings is of the same order
715 of magnitude as the interannual variability of production and is higher than the modeling error.

Finally, poundage power plants fall in an intermediate category, displaying an inter-forcing variability that is 41% lower than the interannual variability.

In conclusion, the uncertainties in precipitation forcing in mountainous regions prove to be critical in the estimation of realistic hydropower potentials for reservoir plants. The calibration carried out relative to SAFRAN is less effective for other forcings (e.g. SAF_COM for instance), as the differences in precipitation data appear as the main contributor to the differences in hydropower potentials.

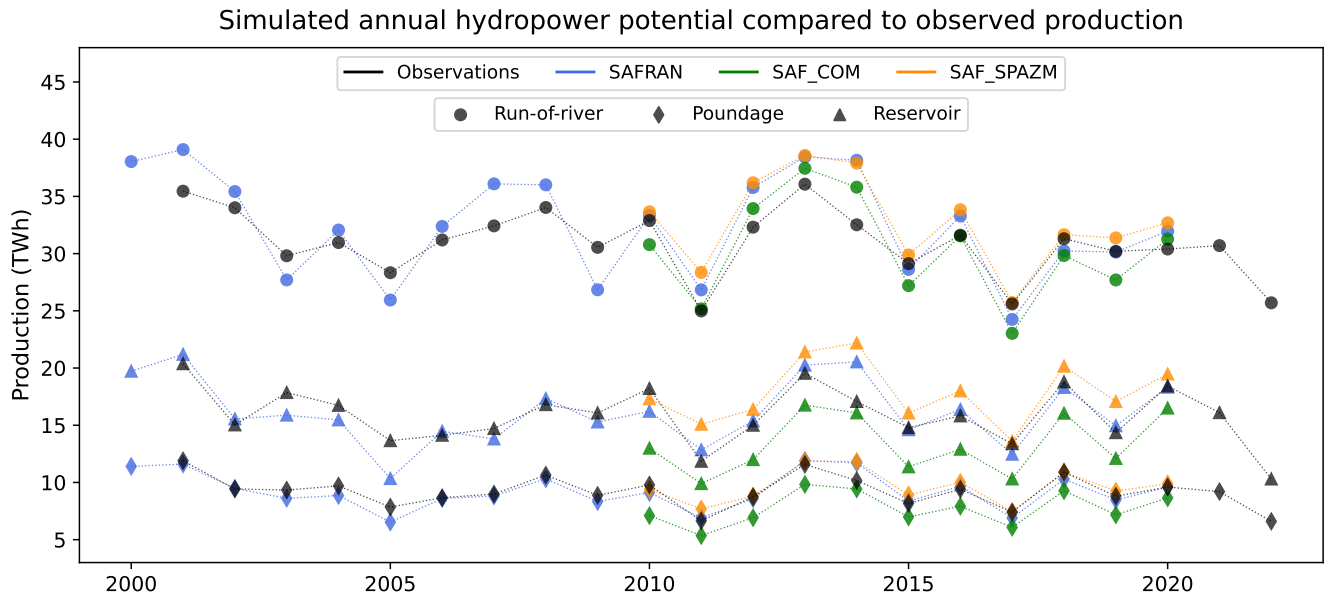


Figure 9. Comparison of estimated annual hydropower potential with observed annual production for the different categories of hydropower plants and for the different atmospheric forcings, after calibration based on SAFRAN.

	Run-of-river		Poundage		Reservoir	
	Calibration Period	Validation Period	Calibration Period	Validation Period	Calibration Period	Validation Period
Mean relative error	-	+ 2.8 %	-	-2.6 %	-	-1.4 %
Mean absolute relative error	3.5 %	6.9 %	3.7 %	5.4 %	2.5 %	7.5 %
Interannual variability (TWh)	3.71		1.71		2.61	
Inter-forcing variability (TWh)	1.32		1.25		2.54	
Modeling error (TWh)	2.64		0.67		1.33	

Table 3. Estimation of the errors in annual potentials prediction

5 Validation of the hydropower simulations

4.1 Hydropower operations

In this section, we assess the model's ability to simulate reservoir management and hydropower production. Observed ~~time-series for each type of hydropower plant (time series of river production (gathering run-of-river production, reservoir production, PHS production and pumping) and poundage power plants) and reservoir production~~ serve as demand inputs for the reservoir operations in the model. At each time step, the model aims to meet this target by operating the reservoirs according to the rules described in Sect. 2.3 and the simulated hydrological cycle. The objective is to verify if our model ~~is able to~~ can simulate operations consistent with observed production ~~and pumping.~~

730 ~~We present here the results obtained from a simulation spanning the period from 2015 to 2020 (period of availability of validation data).~~ 2020.

4.2 Run-of-river production

4.1.1 River production

~~30-minutes run-of-river production observations (RTE, a) include production data from real run-of-river plants that do not have reservoirs, as well as poundage plants associated with small reservoirs. We reproduce this distinction in our model by gathering these two kinds of plants.~~

At each time step, the model first computes the available potential from fatal production (from run-of-river plants and spill or constrained releases from the reservoirs of poundage plants). If this potential falls short of fulfilling the production target, it then operates the reservoirs associated with poundage plants to supplement the production.

740 Figure 10 details how the simulation compares to the prescribed production throughout the period when forced by SAFRAN. The overall seasonality of the production is quite well reproduced, with the model succeeding in meeting the hourly production target 69.0% of the time. The failures ~~(in red in Fig.10)~~ represent a total volume of 6.9% of the prescribed production over the six years. ~~These failures (in red in Fig.10)~~ They mostly occur during ~~Summer and Fall~~ summer and fall and indicate that the simulated hydrology is unable to produce what was actually produced during these periods. In ~~Winter and Spring~~ winter and spring, however, there are instances when the potential of fatal production is higher than the target production (January and February 2018 for instance), which means that, in the model, more power could have been generated during these periods than was actually observed. These discrepancies are likely due to the discharge seasonality bias in the Rhone and Rhine catchments highlighted in ~~Sect. E2, Fig. E4.~~

750 Simulation of run-of-river production in the model, when forced by the alternative forcings SAF_SPAZM and SAF_COM, are presented in Fig. C2 and C4. Using SAF_SPAZM, the failures in meeting the prescribed production are reduced (4.3% of production not satisfied compared to 6.9%), due to slightly higher annual potentials of run-of-river and poundage power plants (Fig. 9). On the other hand, with SAF_COM the lower potentials lead to higher failures (15.4% of the total production),

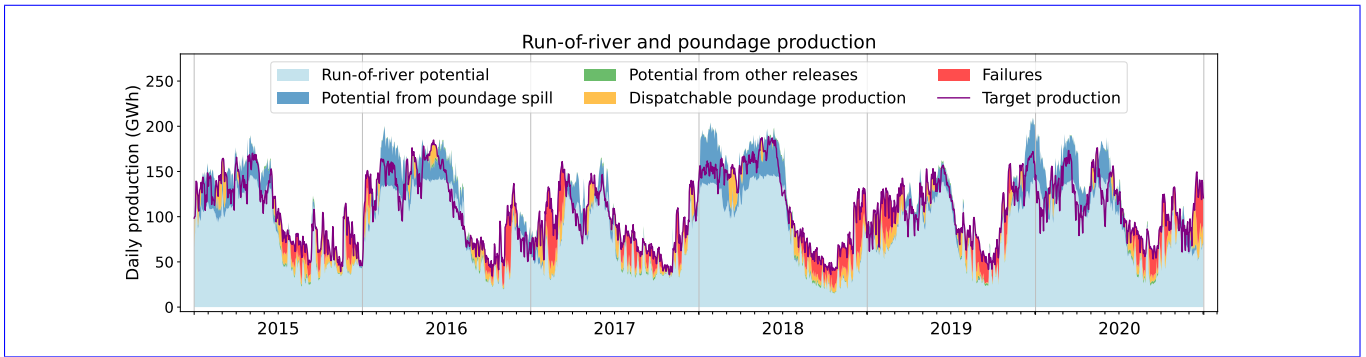


Figure 10. Run-of-river and poundage plants daily production. ~~Purple~~ The purple line indicates the production prescribed to the model and ~~the red coloring~~ shows the ~~difference between this production and failures of~~ the ~~one simulated in the~~ model ~~to meet this target production~~ when forced by SAFRAN. The other colors refer to the nature of the flow that contributes to production in the model. Light blue represents the gross potential of run-of-river plants, dark blue represents the potential of spill from poundage reservoir (water overflowing from the reservoir), green represents the potential from constrained releases of poundage reservoirs and lastly orange represents the dispatchable production, generated by the water specifically released from the poundage reservoirs for power generation.

755 consistent with the lower potentials obtained in Fig. 9. However, the seasonality remains very similar in all three simulations, consistent with the similar seasonality of the simulated discharges for the Rhine and Rhone rivers (Fig. E2).

4.2 Reservoir production

4.1.1 Reservoir production

760 Similarly, ~~30-minutes time-series~~ a 30-minute time series of observed production ~~from by~~ reservoir power plants is prescribed to the model. To fulfill this demand, the model completes the ~~fatal non-dispatchable~~ production that may be available from ~~reservoirs~~ reservoir spillage and constrained releases by operating reservoirs according to ~~the~~ rules defined in Sect. 2.3.

765 ~~The daily reservoir hydropower production simulated under SAFRAN is compared to the historic production in Fig. 11 over the entire simulation period~~ Figure 11 details how the simulation compares to the prescribed production throughout the period ~~when forced by SAFRAN~~. Simulated production under the other forcings ~~are is~~ presented in Fig. C3 and C5. Figure 12 displays the co-evolution of the observed national hydraulic stock (RTE, c) and the one simulated in the model (Eq. (17)) for the three forcings under study.

770 Under SAFRAN, the model successfully meets the production target while simulating hydraulic stock variations consistent with observations throughout the ~~6 years~~. ~~In the model, reservoirs are indeed filled during Spring~~ six-year period. ~~Reservoirs are filled during the spring~~ due to snow melt and depleted during ~~the~~ winter to meet the high electricity demand. ~~Annual variations of hydraulic stock are in line with the discrepancies highlighted in Fig. 9. For example, Fig. 9 shows that the simulated annual potential assuming stock equilibrium is slightly higher than the observed production for the year 2016. Consequently, as we constrain our model to match the observed production, it results in a small volume of water being stored during this year,~~

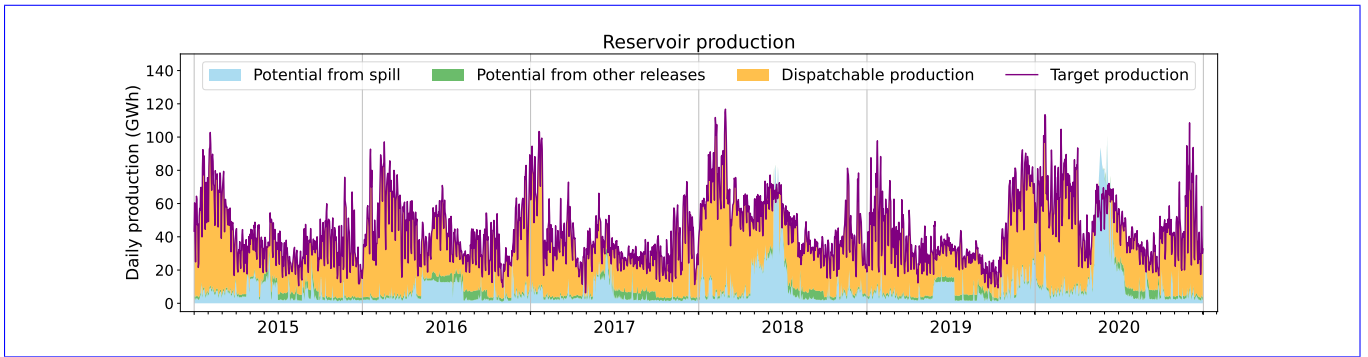


Figure 11. National reservoir plant production simulated in the model. ~~Purple~~ The purple line indicates the production prescribed to the model, while the other colors refer to the nature of the flow that ~~contribute~~ contributes to this production. Blue represents the gross potential from reservoir spillage (water overflowing from the reservoir), green represents the potential from constrained releases of the reservoirs and lastly orange represents the production by the water that is specifically released from the reservoir for hydropower ~~purpose~~ purposes.

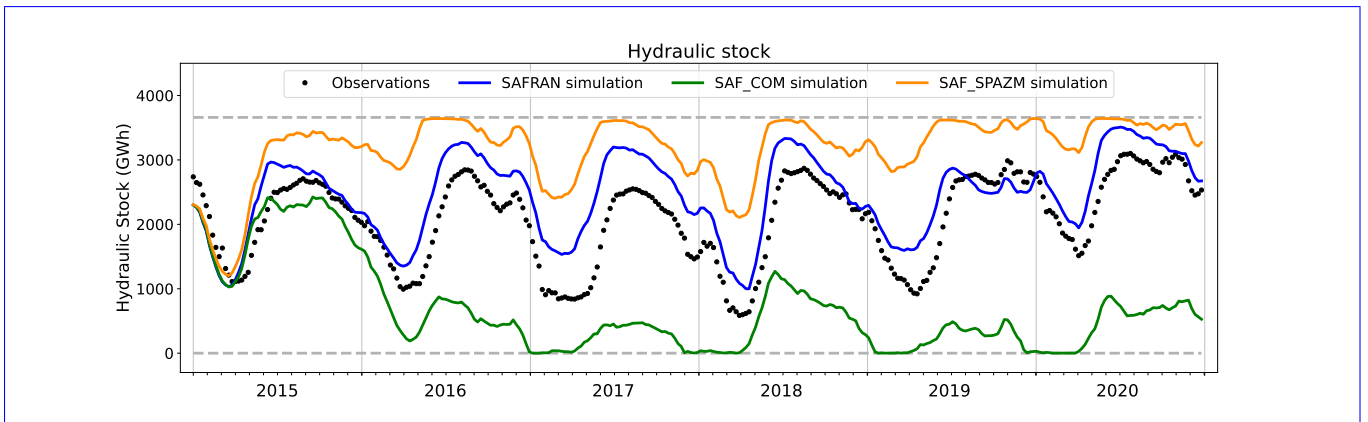


Figure 12. Comparison of national hydraulic stock evolution simulated by the model and weekly observations

leading to a stock higher at the end of the year than at its beginning, which is what we actually observe in Fig. 12. On the contrary, the annual potential simulated assuming stock equilibrium in 2017 is lower than the observed production in Fig. 9, explaining why we simulate a negative annual stock variation over this year (Fig. 12). Nevertheless, a slight temporal shift is observed, as the simulated stock starts to fill some weeks earlier compared to the observations. This temporal shift aligns with the seasonal biases in river discharges identified at the Chamonix Station (Fig. E4), indicating a consistent pattern.

775

Under SAF_SPAZM, the ~~evolution of the simulated stock remains quite satisfactory in comparison to observations, demonstrating a certain robustness of our model relative to changes in precipitation forcings. As shown in Fig. C3, the production potential from reservoir spillage exceeds the target production on multiple occasions (e.g. during May and June 2016)~~ stock remains significantly higher than the observations. Indeed, the simulated annual potential of reservoir power plants exceeds their observed production (Fig. 9), resulting in reduced releases from the reservoirs to meet the prescribed demand. This leads

780

to ~~unused water releases from the reservoir, explaining the negative annual variation of hydraulic stock we obtained for 2016, despite the simulated annual potential being greater than the observed production in 2016 (Fig. 9).~~ high levels of unused spillage, as shown in Fig. C3.

785 Under SAF_COM, however, the stock is completely emptied after the two first years of simulation, and a significant portion of the demand cannot be satisfied (Fig. C5). This is consistent with the huge difference in annual production estimates highlighted in Fig. 9. In addition to the substantial deficit in hydropower potential, a negative feedback loop comes into play. As the reservoir storage diminishes, the head of the power plants decreases, consequently reducing the associated power generation for a given released volume. Consequently, the power plants draw more water to generate the same amount of
790 energy, further exacerbating the decline in reservoir storage. The calibration carried out relative to SAFRAN is not effective ~~to~~ avoid in avoiding this outcome.

Figure 11 allows for the distinction of the different drivers of French hydropower production, depending on the season. In winter, hydropower production is substantial, driven primarily by high electricity consumption. The majority of production stems from intentional reservoir operations, with a minimal proportion attributed to fatal production. In spring, fatal produc-
795 tion becomes more prominent, particularly due to snow melt-induced spillage, resulting in a minimum hourly production, even during periods of low consumption such as at night (only visible at the hourly resolution not displayed here). During summer, although there is no spillage, a significant portion of the hydropower potential comes from constrained ecological and agricultural water releases. When looking at the hourly production (not displayed here), we find a good agreement of between the simulated minimal production with and the observed troughs in RTE's production.

800 4.2 Effects of hydropower operations on river discharges

~~In Sect. E we identified biases in river discharge seasonality, in particular for stations in the Alps (Cheylas station, Fig. E4), which could possibly be attributed to the non-representation of water management.~~ We explore in this section how to what extent the representation of hydropower operations can reduce ~~these biases~~ the hydro-meteorological errors of the model discussed in Appendix E, with the example of two gauging stations located in the Alps. Figure 13 details the location of these
805 stations comparatively to ~~hydropower infrastructures and adduction network.~~ the hydropower network. The Aiguebelle station is located on the Arc river, just upstream of its confluence with the Isère river, and downstream from a series of hydropower plants, including one that generates electricity thanks to through the release of a dam on the Isère river. The Cheylas station is located on the Isère river, downstream of its confluence with the Arc.

Figure 14 compares the seasonality of the discharges simulated at these two locations by ORCHIDEE forced by SAFRAN
810 with and without activating the hydropower operations module.

At Aiguebelle, the representation of this inter-basin water transfer the Aiguebelle station, implementing hydropower operations significantly reduces the annual bias from -31% to -4% (Fig. 14). Indeed, when hydropower operations are activated, part a portion of the Isère's water is diverted from its natural outlet to supply a power plant on the Arc. At Cheylas, no change is observed in the bias of the simulated river discharge.

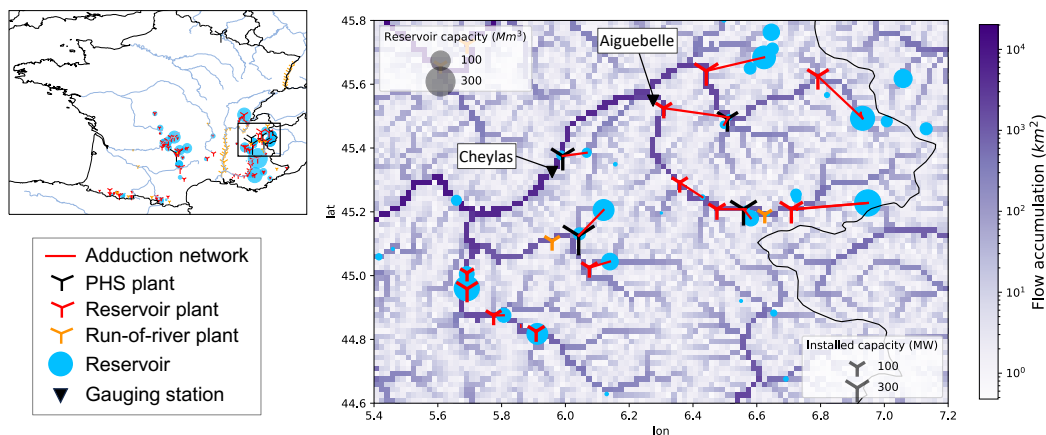


Figure 13. Location of Aiguebelle and Cheylas stations comparatively to hydropower infrastructures in Arc catchment (French Alps). PHS plants are pumped-hydro storage plants not considered in this study.

815 ~~Discharge~~ Furthermore, the discharge seasonality is improved for both stations with higher flows in Fall and Winter due to releases for power generation. ~~The NSE metric is therefore significantly improved~~ This results in a significant improvement in the NSE metric.

We found a similar effect for other French watersheds where flow observations near hydropower plants are available. However, as mentioned earlier, the professional secrecy surrounding French hydroelectric production complicates a systematic and
820 precise evaluation of this improvement in flow simulation.

5 Discussion and conclusion

5.1 A demand-based approach

~~In this study, we demonstrate~~ This study demonstrated the effectiveness of a demand-based approach to simulate hydropower operations in land surface models. The conceptual framework of such an approach ~~is~~ was first described, emphasizing its three
825 original features: (i) the reconstruction of the human-made hydropower network on the model grid to represent not only natural water flows, but also those ~~build~~ built for hydropower management; (ii) the implementation of reservoir operation rules that account for their multi-purpose objectives; (iii) the prescription of an exogenous “hydropower demand” defined at the power grid level to drive the release rules of hydroelectric reservoirs, allowing coordinated management of all hydroelectric resources on the power grid and consistent with power system needs. ~~Then, we explore~~ Subsequently, we assessed the performance of
830 this approach when implemented in the routing module of the ORCHIDEE model, for the case study of the French power grid. ~~ORCHIDEE is run forced~~ The ORCHIDEE model was run driven by an atmospheric reanalysis dataset and national historic hydropower production ~~time-series are~~ time series were prescribed to the model as the hydropower demand to satisfy. ~~We find~~

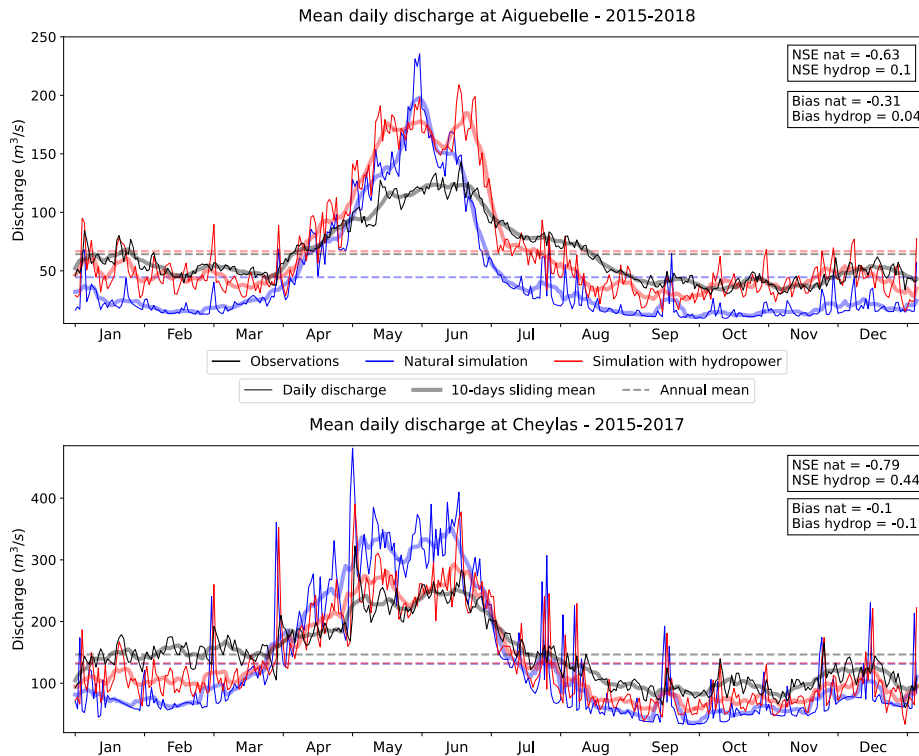


Figure 14. Comparison of daily (fine line) simulated river discharge with hydropower operations (red) and without (blue) and observed discharge (black) for two gauging station-stations in the French Alps. ~~Thicker~~The thicker line is the 10-days-10-day average while the ~~the~~ dashed line is the annual mean.

The results indicate that, when the model is forced to reproduce the historic generation, the implemented method simulates hydroelectric reservoir operations in line with observations of reservoir storage at the national level.

835 Beyond this satisfactory result, our method presents several limitations and opportunities for improvement.

First, the time-series-time series used to drive the reservoirs-reservoir releases in this study is the actual production of dispatchable hydropower plants, which can-may differ from the real demand for dispatchable hydropower production. Indeed, the actual production results-from-is the result of a trade-off between the demand and the prevailing hydrological conditions, particularly the current storage level in reservoirs. If this storage is low, the demand would-not-be-completely-will not be fully
 840 satisfied in order to maintain a certain level for future uses. Besides, we consider an exogenous dispatch of the hydropower production across the different types of hydropower plants (namely run-of-river and reservoir) at each time step. This allows-us to-more-easily-identify-model-weaknesses-approach facilitates the identification of model deficiencies for each type of power plant. For instance, we found a seasonal bias in run-of-the-river hydropower production, that we-would-have-missed-would have been overlooked if a single production target had been used for all power plants. Reservoir-The reservoir plants would
 845 have acted-served as buffers, reducing their production during periods-of excess run-of-the-river output and increasing it during

deficits, so that we would have observed periods of deficits, thereby resulting in discrepancies in the stock evolution. However, in reality, the dispatch of power demand across the different types of hydropower plants is not exogenous but also depends on the hydrological conditions, as the potential for run-of-the-river production being is fully exploited before turning to dispatchable units. To capture these intricate interactions between hydrology and hydropower production decisions, a solution is to
850 couple our model with an economic power system dispatch model (Oikonomou et al., 2022). This coupling would ensure that the power demand dispatch used to drive reservoir operations in ORCHIDEE considers the hydrological states simulated within the ORCHIDEE model. If This would result in a comprehensive modeling framework wherein simulated hydropower production simultaneously adheres to constraints related to water availability, non-power reservoir operations, and minimization of power system costs. In particular, hydropower demand would be endogenously adjusted to match the hydropower potentials
855 of the simulated hydrology, and could avoid entering the feedback loop where reservoirs are emptied, as in the SAF_COM simulation. This novel approach holds significant promise-promises for enhancing the consistency and realism of hydropower production simulation, in particular the study of the joint impacts of climate change and variable renewable energy integration.

Second, in this study, we opted for a simple rule to distribute national production among different power plants and demonstrated that such a rule can-could simulate credible hydroelectric operations at the national level. As no time-series-time series
860 of production is available at the individual plant level in France, the realism of the simulated individual operations is difficult to assess. This choice can, however, be further investigated, in particular by testing alternative distribution rules, such as those proposed by Lund and Guzman (1999). Additionally, the operations we simulate assume that a social planner controls the entire grid's power plants and reservoirs, optimizing the collective production. In reality, power plants may belong to different stakeholders, each seeking to maximize their profit. Ambec and Doucet (2003) have shown that such decentralized manage-
865 ment can lead to suboptimal resource management, which could not be reproduced by the proposed model. However, in the case of France, our assumption is justified as the historical production company, EDF, owns nearly 85% of the hydroelectric production.

Third, as we focused primarily on hydroelectric usage, other water uses are simplified or even absent in the current version of our model. Specifically, no water abstraction for domestic, industrial, or agronomic needs is included in our model. Following
870 Zhou et al. (2021), the irrigation demand could be explicitly calculated by the model based on the deficit between potential evaporation and actual evapotranspiration. In other studies, domestic and industrial water demands are estimated using socio-economic proxies such as population density or GDP (Neverre, 2015).

~~As mentioned in the introduction, process-based hydrologic models forced by future climate projections have been used to project the evolution of annual hydropower production at a national or regional scale (Van Vliet et al., 2013; Liu et al., 2016; Voisin et al., 2017). By differentiating the place of water abstraction from the place of power generation, our new method offers opportunities to improve the estimation of such annual potentials. To accurately assess the resilience of power grids to a different climate, a realistic representation of daily and hourly hydropower operation is required. In most previous hydropower studies, hourly hydropower production is calculated based on reservoir releases that follow generic rules, independently of the specificity of hydropower reservoirs (Abeshu et al., 2023). Our method instead, allows hydroelectric dams to be specifically operated, in line~~

875

880 ~~with hydroelectric demand, and thus improving the representation of the hourly production of dispatchable hydropower plants.~~

5.2 Sources of uncertainties

We have paid particular attention to ~~identify and discriminate~~ identifying and discriminating among the various sources of uncertainty that may affect the estimation of hydroelectric production using such a method. ~~We demonstrate that,~~ Our findings
885 indicate that while errors in simulated discharge are ~~predominant for~~ prevalent in most watersheds in our case study, ~~our~~ the limited knowledge of the hydroelectric adduction network is the main source of uncertainty for hydropower infrastructures in mountainous basins. To our knowledge, no dataset comprehensively documents these complex "hydroelectric links", which operate on a small scale. Therefore, an in-depth analysis of the gray literature released by the various stakeholders is necessary to reconstruct this network in detail. ~~We nevertheless propose~~ Furthermore, we proposed a calibration method to overcome
890 this limitation ~~, and validate and validated~~ it against observations for the case study of France. This method can therefore be extended to countries with ~~little~~ limited information available on the hydroelectric network.

Regarding hydro-meteorological errors, the use of three different precipitation datasets allows us to understand their more precise origin. In several watersheds crucial for hydroelectricity (such as Durance or Lot), and especially in the upstream parts, uncertainties in observed precipitation appear to be the primary contributor to the error in simulated discharge. On the Rhone
895 or the Rhine rivers, on the contrary, errors in the simulated discharges seem to stem more from processes not represented in the model (such as water withdrawals for human uses, for example). Though incomplete, this work contributes to the current effort to integrate human water management into hydrological models, in order to simulate a more realistic water cycle (Nazemi and Wheeler, 2015a). We show that our method can improve river flow simulations in some mountain catchments where hydropower cannot be neglected.

900 Finally, our study shows that comparing hydropower estimates with observed production offers an indirect means of checking the quality of meteorologic data. In our study case, we demonstrate the lower quality of the COMEPHORE dataset in mountainous regions compared to SAFRAN or SPAZM, something already identified by Birman et al. (2017); Magand et al. (2018).

5.3 Perspectives

905 In conclusion, the demand-based operations proposed in this study hold promising prospects for enhancing our understanding of the resilience of different power mix scenarios to changes in climate, water management, or land use. The next steps in this trajectory involve (i) integrating our climate-based hydropower model with a power system model to get a comprehensive framework that captures all relevant constraints on hydropower production, (ii) applying this integrated framework to climate change scenarios and power system scenarios to assess the adaptive capacity of the power grids, and (iii) refining the description
910 of other water uses to more completely describe the competition for water resources.

Code and data availability. The ORCHIDEE version developed for this project is available upon request. The meteorological forcings used in this study were provided by Meteo-France for SAFRAN (<https://www.umr-cnrm.fr/spip.php?article788&lang=en>) and COMEPHORE (<https://radarsmf.aeris-data.fr/en/home-page/>), and EDF-DTG for SPAZM (Gottardi et al., 2008)). The observed data used for validation is openly accessible online. River discharge data can be downloaded at <https://hydro.eaufrance.fr/>, while data on energy production is available at <https://opendata.reseaux-energies.fr/>. The reservoir dataset was built based on the GRanD database (Lehner et al., 2011), which can be found at <https://www.globaldamwatch.org/grand/>, and on the data of the *Comité Français des Barrages et Réservoirs* (CFBR) at <https://www.barrages-cfbr.eu/-En-France->. Finally, the plant's database was built from the EU JRC hydro-power plants database (<https://github.com/energy-modelling-toolkit/hydro-power-database>) and the *Registre national des installations de production raccordées au réseau de transport d'électricité*, which can be downloaded at <https://opendata.reseaux-energies.fr/>.

915

A1 Locating hydroelectric infrastructures on the river network

Dams and hydropower plants are located on the MERIT grid based on geo-referenced and upstream area information provided in the databases (Infrastructures datasets used for our study over France are presented in Appendix B). The location procedure is done following these steps:

- 925 1. We identify a first location based on the infrastructure's geographical coordinates.
2. We define a search area around this first location (typically 10km)
- If the upstream area of the infrastructure is informed in the databases, we identify all the pixels in the search area having an upstream area close enough to the one being searched (typically +/- 20%) and, among these eligible pixels, the one closest to the first location is selected. If no pixel checks this condition, the infrastructure is not
- 930 placed.
- Otherwise, we look for the closest pixel to the first location likely to be positioned on a river. To do this, the maximum upstream area of the pixels in the search area is identified (U_{max}) and the closest pixel to the first guess pixel satisfying ($U > \frac{U_{max}}{10}$) is selected, with U being the upstream area of the pixel.

Note that each vertex and edge can respectively contain only one dam or hydropower plant. If several reservoirs are placed

935 on the same HTU during pixel aggregation, their respective volumes for the different uses are summed. If two plants are placed on the same edge, their installed power and pumping capacity as well as their head are summed only if both plants have the same input point. Otherwise, only the plant with the highest installed capacity is kept. As in other studies (Abeshu et al., 2023), all the reservoir attributes are associated with the HTU of the dam (even if its water surface can be larger than the HTU area and its geometry is different from the HTU geometry).

940 **A2 Adduction network**

Poundage and reservoir plants generate electricity from the water released from the upper reservoirs. To explicitly represent this adduction network in our model, we have to identify such connections between a feeding reservoir and a power plant. Since datasets describing these connections are rarely available, we use an algorithm to identify these connections. For each poundage or reservoir plant, we thus select as the feeding reservoir the one that maximizes the potential function $\phi = \frac{U*V*h}{d}$, where U is the upstream area of the dam, V is the storage capacity of the reservoir, h is the elevation difference between the plant and the reservoir and d is the horizontal distance between them. The definition of these potential functions is inspired by similar works aiming to connect an irrigated area to a water supply point (Neverre, 2015; Zhou et al., 2021).

945

This position algorithm relies on the assumption that each plant is fed by only one reservoir. This assumption is however debatable, especially for plants in mountain areas that may be connected to several reservoirs. In this case, our choice of the potential function ϕ privileges the reservoir with the largest upstream area since it is likely to determine the production potential

950

of the plants. During calibration (see Sect. 2.5), plants for which the identification of a single reservoir conducts to a significant misrepresentation of the plant's hydropower potential are identified and a correction is made by moving the withdrawal point so that it gathers enough water to ensure the observed production is possible.

Appendix B: Datasets

955 B1 Dams and reservoirs

We use global reservoir data from GRanD (Global Reservoirs and Dams) dataset (Lehner et al., 2011), that-which gathers data of large reservoirs and dams worldwide (volume $> 0.1km^3$, hence a total of 7320 dams). The database contains 137 dams in France, 63 of which are used for hydroelectricity. However, some important dams for French hydroelectricity are not documented in this database. Therefore we completed the database for this study with data from the CFBR (Comité Français des Barrages et des Réservoirs), which is in charge of the inventory of French dams higher than 15m for the ICOLD (International Commission on Large Dams). We extracted data from its website <https://www.barrages-cfbr.eu/> (CFBR, 2021) to complete the GRanD database. Our database finally gathers 492 French dams (Metropolitan France). Their location, original database, and intended purposes are shown in Fig. B1.

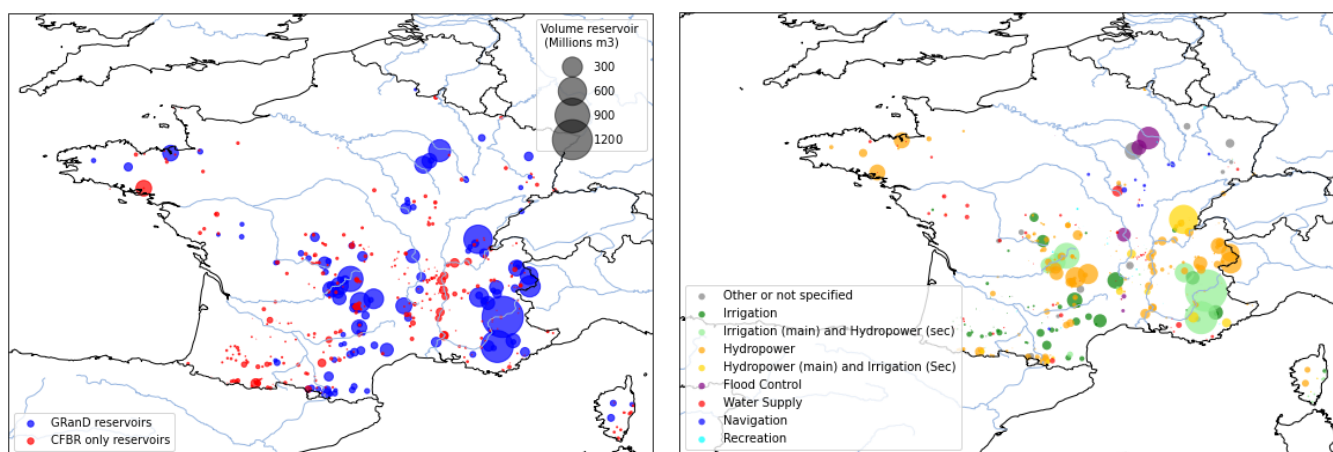


Figure B1. Location and main uses of the reservoirs in the final database

B2 Hydropower plants

965 ~~We use hydropower plants data~~ The data used in this study are obtained from the EU Joint Research Center (JRC) Hydro-power plants database (European Commission and Joint Research Centre (JRC), 2019). This database gathers geographical coordinates, installed power capacity, plant type (run-of-river, reservoir or pumped-storage), or PHS), and hydraulic head for 4186 European plants (for a total installed capacity of 161 ~~GW~~GW). 153 of these plants are located in France, representing 20.6 ~~GW~~.

970 GW. Other available datasets of French hydropower plants are the national registers of electricity generation and storage facilities published annually (ODRÉ, 2016, 2018). The 2016 register gathers data from 414 hydropower plants ~~for~~, with a total installed capacity of 23.4 ~~GW~~GW. However, as these registers do not provide the geographical coordinates of the plants, we chose to use the RTE-2016 national register to ~~correct~~ rectify head information

and classify-categorize the plants in the 4 categories used by the French operator: run-of-river, poundage (intermediate-category-between-run-of-river-and-reservoir), reservoir and pumped-storage. Fig. reservoir, and PHS. Figure B2 shows the locations of the different plants included in out-final-database our final database, while Table B1 summarizes the differences-discrepancies between the databases in terms of installed capacities. Its last line details the main features of the final database we use for this study.

	Total	RoR	Poundage	Res.	PHS (prod)	PHS (pump)
National Register 2016 (ODRÉ, 2016)	23.426	5.943	3.715	8.748	4.965	4.591
JRC (initial categories)	19.695	5.87	-	8.76	5.06	4.84
Final database (JRC with RTE categories placed on HTUs) (compared to ODRÉ (2016))	19.638 (84.6%)	4.426 (74.2%)	2.606 (71.7%)	7.434 (86.0%)	5.05 (100%)	4.84 (100%)

Table B1. Comparison of the different databases in terms of installed hydroelectric capacities (GW) in metropolitan France (without Corse et DOM-TOM)

B3 Conversion factors for hydropower generation

980 As presented in Table B1, our final dataset does not include all the hydropower plants installed in France. However, using annual production data of each plant provided by ODRÉ (2015, 2016, 2018), we can quantify the share of the national production provided by the power plants in our database. This enables us to compute a factor to convert the actual production of national time-series (RTE, a) into representative production in our model both for prescribing the production demand and comparing the results. The computation of such conversion factors is presented in Table B2. It relies on the assumption that within each
 985 category of power plant, the geographical distribution of plants in our database is representative of all French power plants so that production ratios remain constant over time. This assumption is debatable as our database includes the largest power plants in terms of installed capacity, which are predominantly concentrated in certain regions, while smaller-scale plants may be located in watersheds not represented in our database (e.g., run-of-river plants on the River Seine for instance). However, as the missing plants have, by definition, a lower installed capacity than those in our database, their contribution to national
 990 production is lower and can reasonably be neglected.

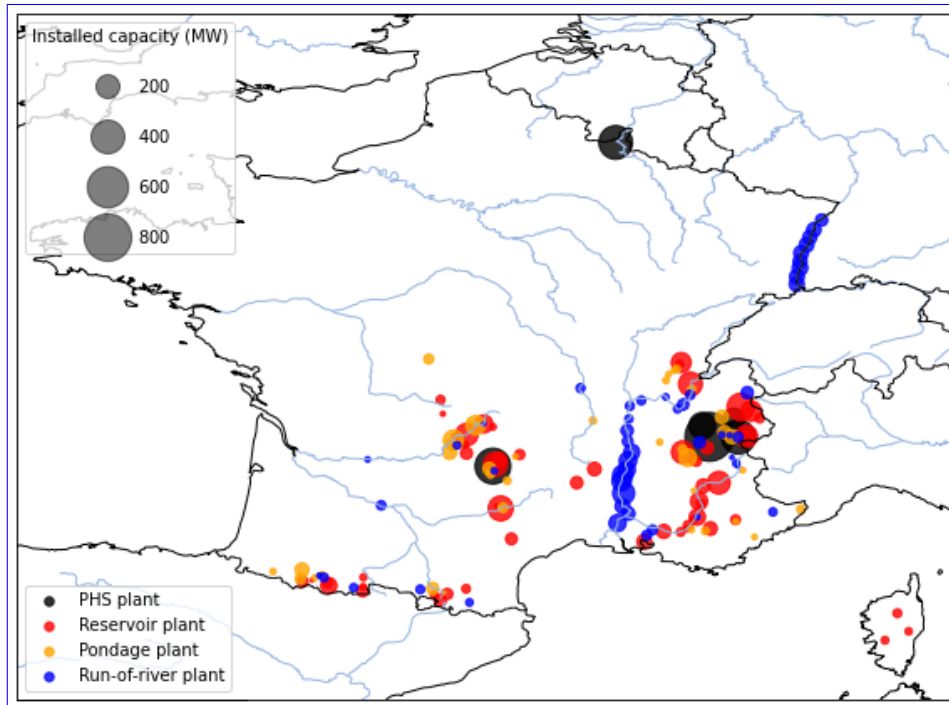


Figure B2. Typology of the plants in the database

	Total	RoR	Poundage	Res.	PHS (prod)	PHS (pump)
RTE 2016 (RTE et al., 2016)	62.6	31.6	9.4	15.8	5.8	6.7
National Register 2016 (ODRÉ, 2016)	57.6	27.5	9.0	15.6	5.8	n.a.
(compared to RTE et al. (2016))	(92.0%)	(87.0%)	(95.7)	(98.7%)	(100%)	n.a.
Production plants in database 2016 (based on ODRÉ (2016))	47.9	22.4	5.5	14.1	5.9	n.a.
Coefficients 2016		70.9%	58.5%	89.3%	100%	n.a.
RTE 2018 (RTE et al., 2018)	66.9	31.3	10.9	18.8	5.9	7.4
National Register 2018 (ODRÉ, 2018)	60.7	26.4	10.0	18.3	6.0	n.a.
(compared to RTE et al. (2018))	(90.7%)	(84.3%)	(91.7%)	(97.3%)	(100%)	n.a.
Production plants in database 2018 (based on ODRÉ (2018))	48.1	20.5	6.0	16.2	5.9	n.a.
Coefficients 2018		65.5%	55.0%	86.1%	100%	n.a.
Conversion factors		68.2% %	56.8%	87.7%	100%	

Table B2. Comparison of the different available databases in terms of annual production (TWh) and calculation of conversion factors.

n.a.=not available

Appendix C: Alternative precipitation datasets

C1 Presentation of the datasets

C1.1 COMEPHORE

995 COMEPHORE (COMbinaison en vue de la Meilleure Estimation de la Précipitation HORaiRE) dataset provides observations of surface precipitation accumulation over metropolitan France at an hourly and kilometeric resolution based on a synthesis of radar and rain gauge data. A specific processing chain has been implemented in order to address the various sources of error affecting radar data, in particular its low quality in high altitude mountainous areas like the Alps or the Pyrenees (Fumière et al., 2020). The final database is nevertheless assumed to be the best representation of surface precipitation over metropolitan France (Fumière et al., 2020).

1000 We build a meteorologic dataset SAF_COM by replacing precipitation data in SAFRAN with data from COMEPHORE. As COMEPHORE does not distinguish solid and liquid precipitations, we keep SAFRAN's hourly ratio of solid/liquid precipitations when possible and discriminate based on the air temperature otherwise.

The differences in annual mean precipitation are generally small between SAFRAN and COMEPHORE, with an average deviation inferior to 1.0% in COMEPHORE compared to SAFRAN (Fig. C1). However, we find a small seasonal bias as this average deviation goes from -2.0% for the Winter period to +1.9% in the Summer. Moreover, discrepancies increase dramatically in mountainous regions, especially in the Alps and the Pyrenees. For grid points with an average elevation above 1000m, the annual mean precipitation in COMEPHORE is, on average, 10.4% lower.

C1.2 SPAZM

1010 SPAZM (SPAtialisation des précipitations en Zone de Montagne) is a daily reanalysis of precipitation at the kilometer scale, developed by EDF, the main electricity producer in France. SPAZM specifically covers the southern half of the French territory, where a large majority of hydroelectric power plants are located (Gottardi et al., 2008). Climatological precipitation outlines are first constructed based on daily precipitation observations categorized by types of oceanic circulation (weather patterns) (Garavaglia et al., 2011). These outlines are then spatially interpolated onto the kilometer-scale grid and deformed daily according to available observations. In addition to Météo-France's observations, which are also used to construct SAFRAN, EDF's measurement network is utilized. We interpolate the daily precipitation data from SPAZM to the hourly scale and merge it with SAFRAN data to create the alternative forcing dataset SAF_SPAZM. As for SAF_COM, we keep SAFRAN's hourly ratio of solid/liquid precipitations when possible. Compared to SAFRAN, precipitations are in average 2.7% higher in SPAZM with an average bias of 7.0% in Summer, against 2.1% in Winter. Bias is heterogeneously spread over France (Fig. C1) with bigger differences on the highest reliefs, without a clear sign (average deviation of +3.9% for grid points above 1000m).

1020

Average relative bias (%) in total precipitation compared to SAFRAN (2010-2020)

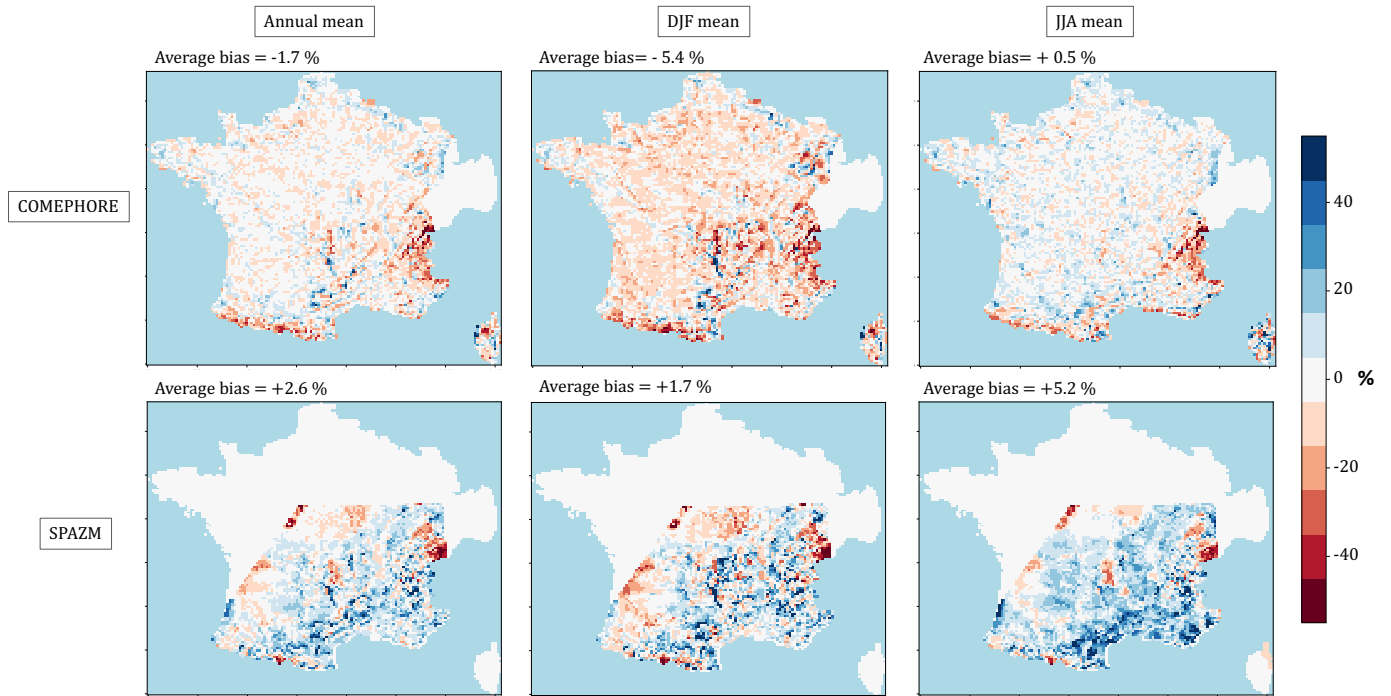


Figure C1. Average relative differences in total precipitation across the datasets for the period 2010-2020.

Left column: annual average bias, middle: average bias in Winter period (December-January-February), right: average in Summer period (June-July-August)

Top: COMEPHORE dataset compared to SAFRAN, Bottom: SPAZM compared to SAFRAN

C2 Simulation of hydropower production under SAF_SPAZM

C3 Simulation of hydropower production under SAF_COM

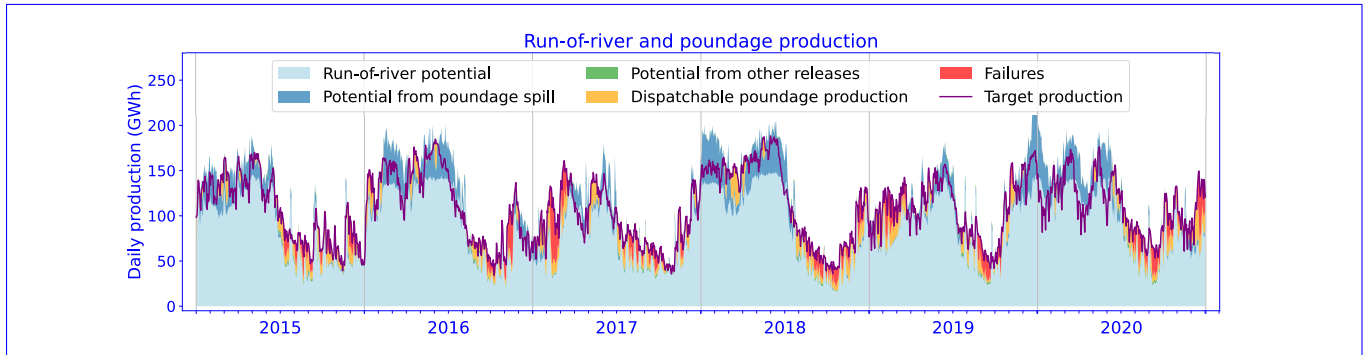


Figure C2. National run-of-river plant production simulated in the model when forced by SAF_SPAZM. The purple line indicates the production that has been prescribed to the model and the red shows the difference between this production and the one simulated in the model when forced by SAF_SPAZM. The other colors refer to the nature of the flow that contributes to the production in the model. Light blue represents the gross potential of run-of-river plants, dark blue represents the potential of spill from poundage reservoir (water overflowing from the reservoir), green represents the potential from constrained releases of poundage reservoirs and lastly orange represents the dispatchable production, generated by the water specifically released from the poundage reservoirs for power generation.

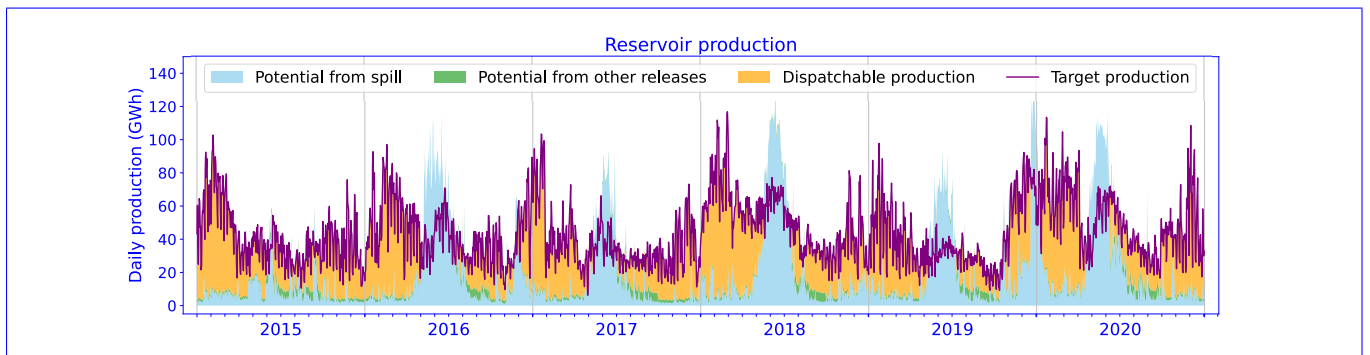


Figure C3. National reservoir plant production simulated in the model when forced by SAF_SPAZM. The purple line indicates the production that has been prescribed to the model. The other colors refer to the nature of the flow that contributes to this production. Blue represents the gross potential from reservoir spill (water overflowing from the reservoir), green represents the potential from constrained releases of the reservoirs and lastly orange represents the production by the water that is specifically released from the reservoir for hydropower purposes.

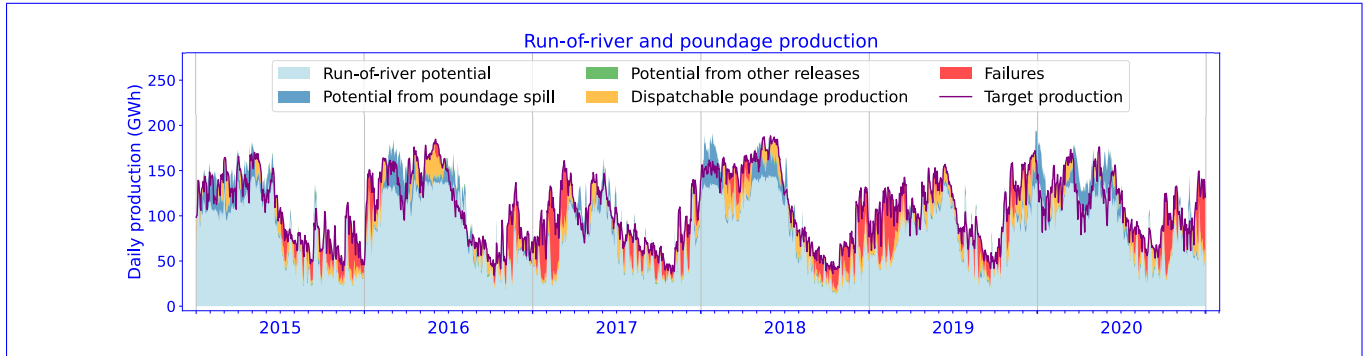


Figure C4. National run-of-river plant production simulated in the model when forced by SAF_COM. The purple line indicates the production that has been prescribed to the model and the red shows the difference between this production and the one simulated in the model when forced by SAF_COM. The other colors refer to the nature of the flow that contributes to the production in the model. Light blue represents the gross potential of run-of-river plants, dark blue represents the potential of spill from poundage reservoir (water overflowing from the reservoir), green represents the potential from constrained releases of poundage reservoirs and lastly orange represents the dispatchable production, generated by the water specifically released from the poundage reservoirs for power generation.

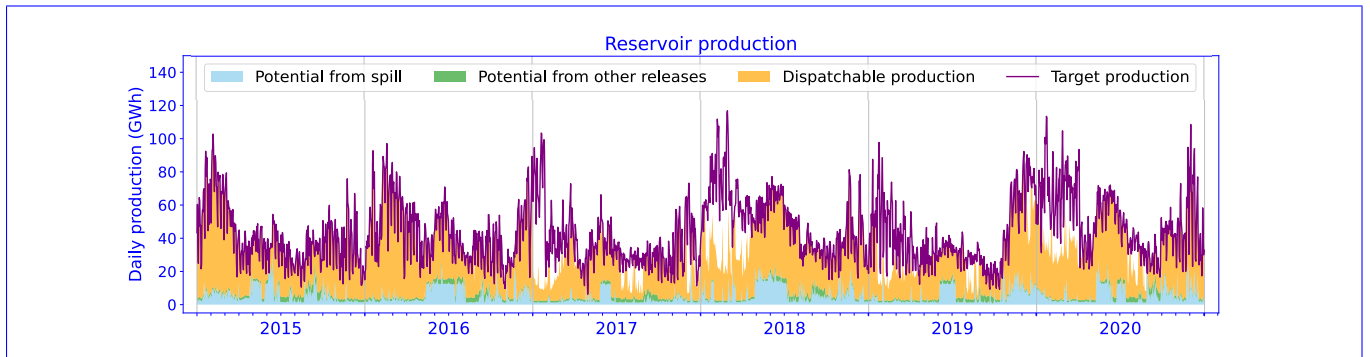


Figure C5. National reservoir plant production simulated in the model when forced by SAF_COM

Purple line indicates the production that has been prescribed to the model. The other colors refer to the nature of the flow that contributes to this production. Blue represents the gross potential from reservoir spill (water overflowing from the reservoir), green represents the potential from constrained releases of the reservoirs and lastly orange represents the production by the water that is specifically released from the reservoir for hydropower purpose.

Appendix D: Hydropower network error

1025 The La Bathie power plant is the most important reservoir hydropower plant in France in terms of installed capacities. It is located in the Alps and fed by numerous water intakes ~~represented~~, as illustrated in Fig. D1. Among them, are the reservoirs of Roselend, Saint Guérin, and La Gittaz as well as other intakes directly connected to rivers or glaciers.

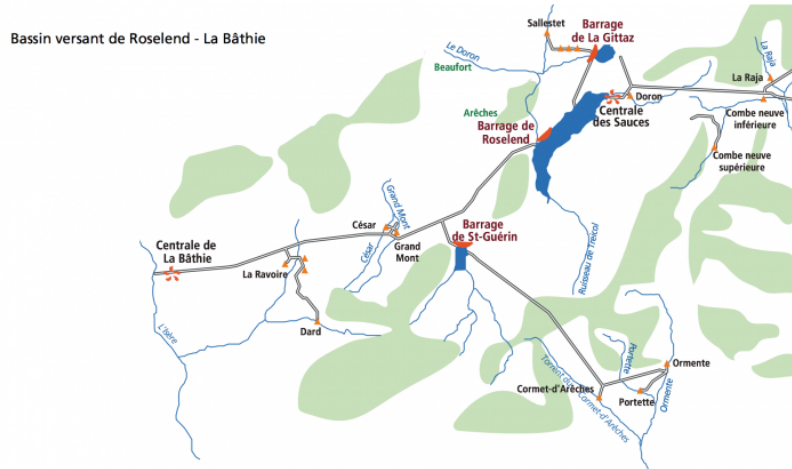


Figure D1. Schematic representation of the water aduction network to La Bathie power plant (source:vpah-auvergne-rhone-alpes.fr)

Figure D2 describes the same area in HTUs space :-

1030 ~~We see in Fig. D2 that Roselend reservoir account and shows that the Roselend reservoir accounts~~ for only a small part of the water being transferred to the hydropower plant. ~~Nevertheless, as no systematic database gathers data on hydropower plants water intakes, we keep our method to select the main reservoir as water input and then slightly moving it in order to account for~~

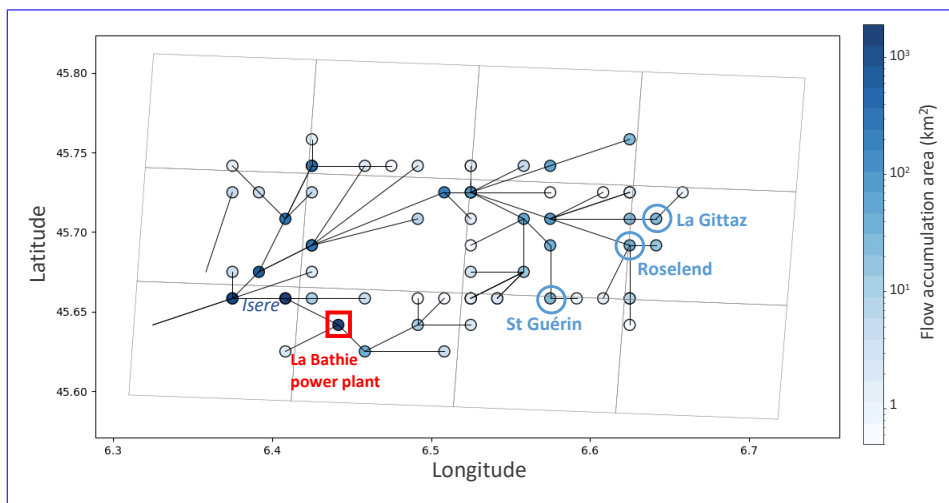


Figure D2. HTUs representation in the model for the same spatial area as Figure D1. The location of hydropower infrastructures is indicated.

Appendix E: Hydro-meteorological errors

To evaluate the performance of the ORCHIDEE model to simulate river discharges in France, independent of reservoir operations, we compare daily river discharges simulated by the model with the observations database of Schapi (2022). It is important to acknowledge that the observed discharge data represents actual discharge values, including water withdrawals, while at this stage, our model generates natural discharges without such withdrawals and dam operations.

E1 Bias in average discharge

Figure E1 displays relative biases of average discharge simulated by ORCHIDEE forced by SAFRAN over the 2010-2020 period for a selection of gauging stations located on rivers equipped with hydropower infrastructure (see Fig. B2 for the detailed locations of the power plants). We chose the bias metric because the annual mean discharge is the most relevant parameter for hydropower potential.

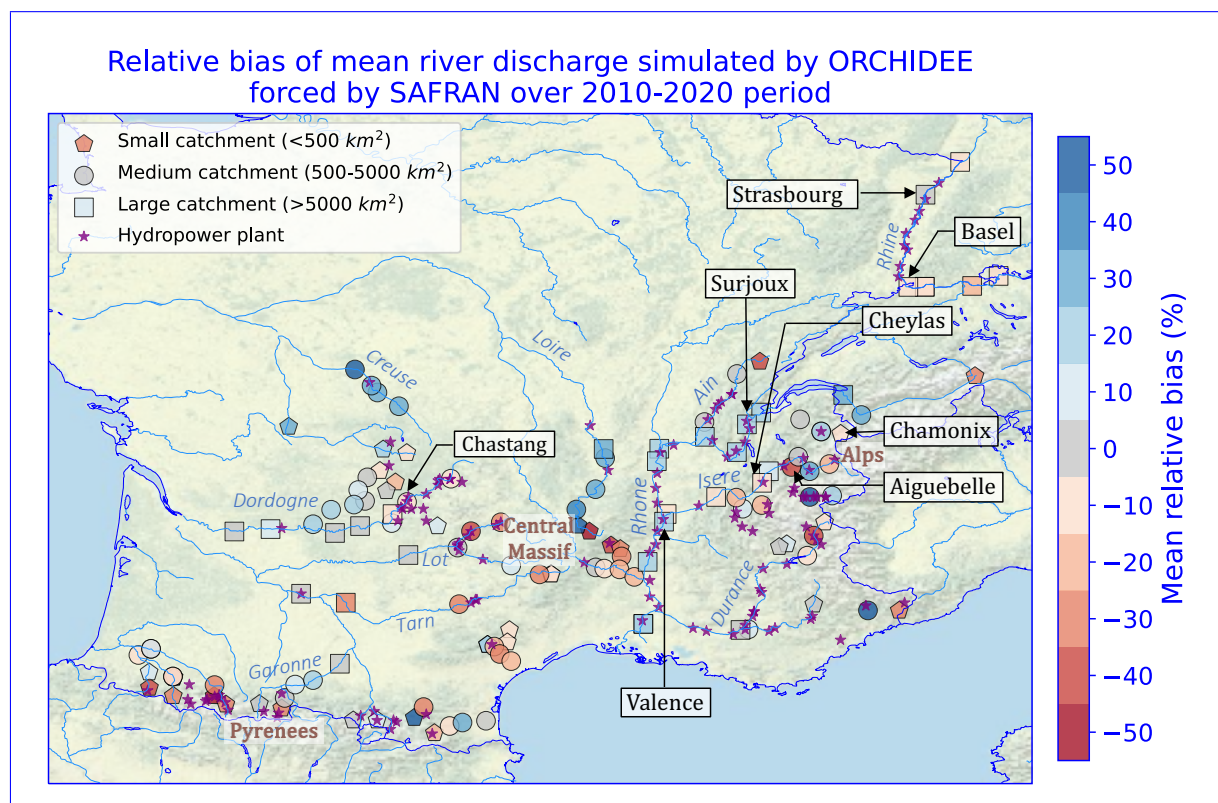


Figure E1. Relative bias of average discharge for a selection of gauging stations located on French rivers equipped for hydropower for the period 2010-2020. Each colored point represents a gauging station. The shape indicates the size of the concerned watershed while the color indicates the calculated bias at this location. Purple stars indicate the locations of the hydropower plants located on the grid.

Source: authors, based on a layer by U.S. National Park Service

The overall performance of the model indicates a slight overestimation of flows, with an average bias of +2.4%.

1045 The discharge bias shows an increasing trend with the upstream area of stations. For small catchments (less than 500 km²), the average bias is -1.6%. In medium-sized catchments (between 500 and 5000 km²), the bias decreases to +1.1%. In large catchments (more than 5000 km²), the bias becomes more pronounced, reaching 7.6%. It is however important to note that the smaller the upstream area, the greater the uncertainty in the location of the station. In Fig. E1, only the stations located with an error in the upstream area lower than 20% are displayed.

1050 On the largest rivers (Rhine and Rhone), where most run-of-river power plants are located, the bias shows little spatial variability, constant at around +20% for the Rhone and -10% for the Rhine respectively. In the Alps, on the other hand, where a significant proportion of dispatchable hydroelectric capacity is installed, the bias displays a high spatial heterogeneity, sometimes within the same river. Upstream of the Isere river, the bias varies from -19% to +26% between two stations some twenty kilometers apart. The upstream reaches of the Durance also show negative biases.

In the other massifs equipped for hydroelectricity (the Pyrenees and Massif Central), there are also negative biases at altitude, which gradually diminish downstream.

1055 Assuming negligible observational errors, discharge bias can originate from different error sources:

- Errors in the atmospheric forcing applied to ORCHIDEE;
- Modeling errors in the energy, water, and carbon cycles;
- Missing processes in ORCHIDEE like glacier melting, interactions with groundwater, and water withdrawals).

1060 To explore the first hypothesis, Fig. E2 compares discharges simulated by ORCHIDEE using the two alternative forcings (SAF_COM and SAF_SPAZM) with the reference SAFRAN simulation. The relative biases of these simulations to observations are presented in Fig. E3.

1065 Under SAF_COM, simulated discharges show relatively small differences on annual average, except in mountainous watersheds (Alps and Pyrenees), where the lower precipitation in COMEPHORE results in streamflows that are 30% to 40% lower when compared to the SAFRAN simulation. However, a pronounced seasonal pattern is observed. The simulated streamflows in winter are lower in the simulation forced by COMEPHORE across France (averaging -16% and up to -50% for the Loire and Durance rivers), while in summer, they are higher (averaging +25% and up to +50% for the Loire River). As regards comparison with observed flows (Fig. E3, the negative biases existing under SAFRAN in the Alps and Pyrenees are accentuated, particularly along the Durance and Isere rivers where many hydroelectric power plants are located. However, for some Alpine stations and the Massif Central, for which the flow is overestimated with SAFRAN, the flow is more accurately simulated with COMEPHORE.

1070 Under the SAF_SPAZM forcing, river discharges show an increase in the majority of watersheds, which is consistent with the previously highlighted higher precipitation in this dataset. However, the upper Rhone watershed stands out with a decrease in simulated discharge, reaching up to -40% during the summer season, allowing for a reduction in the bias of simulated discharges in this area.

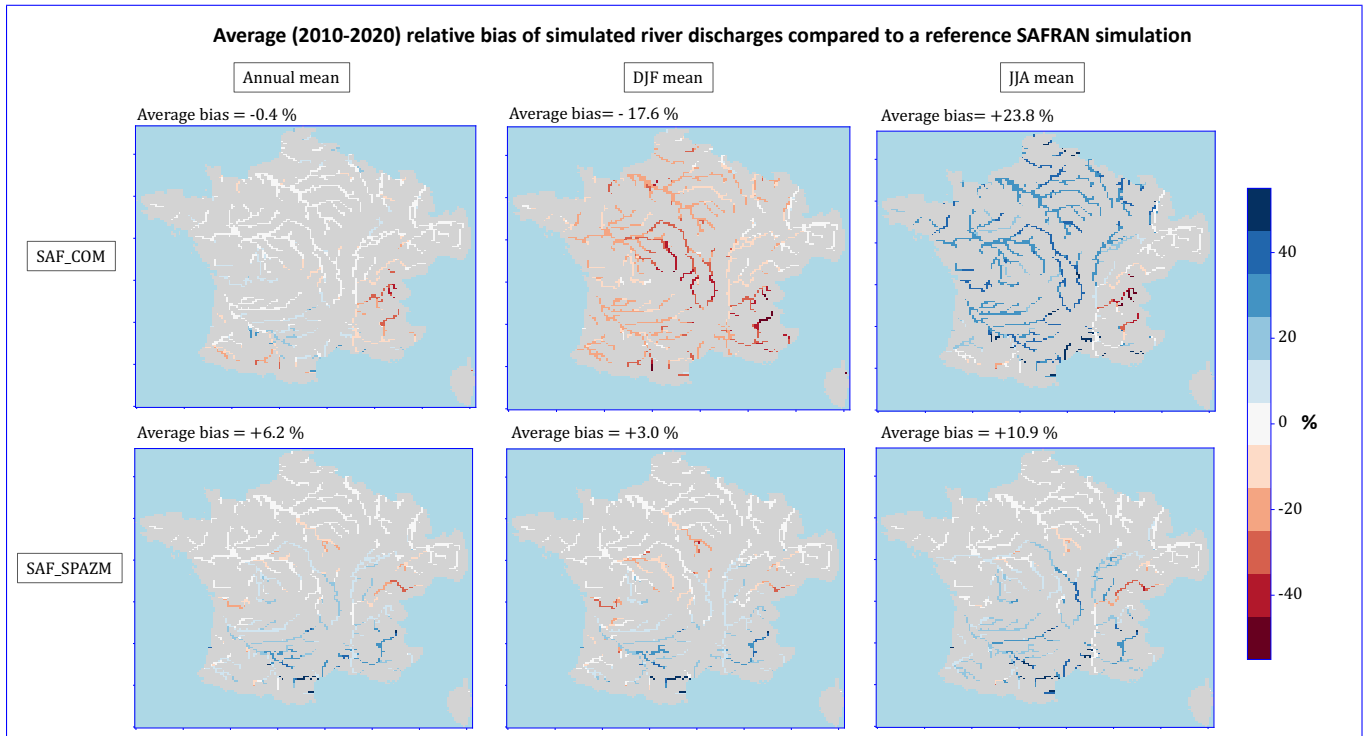


Figure E2. Average relative bias in discharge simulated by ORCHIDEE under alternative precipitation forcings. Results are given in relative difference compared to the reference SAFRAN simulation, for the period 2010-2020. Left: annual average bias, middle: average bias in the Winter period (December-January-February), right: average in the Summer period (June-July-August). The discharges are displayed for all grid points with an upstream area higher than 1000 km^2 .

1075 Even if we limit our analysis to the ~~other water inputs~~ precipitation variable without considering other forcing variables, we show a significant influence of the forcing variability on the simulated discharges.

E2 Discharge seasonality

Beyond the bias in average values, the performance of ORCHIDEE in reproducing the seasonality of the discharge is key for the modeling of run-of-river production as well as that of poundage power plants, which have only a very limited storage capacity. Observations and simulations of daily discharges under SAFRAN forcing are presented in Fig. E4 for selected gauging stations in catchments equipped with run-of-river or poundage power plants.

1080 As depicted in Fig. B2, run-of-river plants are mostly located along the Rhone and Rhine rivers. In the upper Rhone (Surjoux station), there is a substantial overestimation of high flows and an underestimation of low flows. The error reduces progressively downstream: the Nash Sutcliffe efficiency (NSE) is better at the Valence station, despite a higher overall annual bias (likely due to the non-representation of water withdrawals). On the Rhine (Basel and Strasbourg stations), we see similar errors, with an underestimation of low flows during the Fall and an underestimation of the Spring maximum. The discrepancy in the Rhone's

Relative bias of mean river discharge simulated by ORCHIDEE forced by alternative forcings over 2010-2020 period

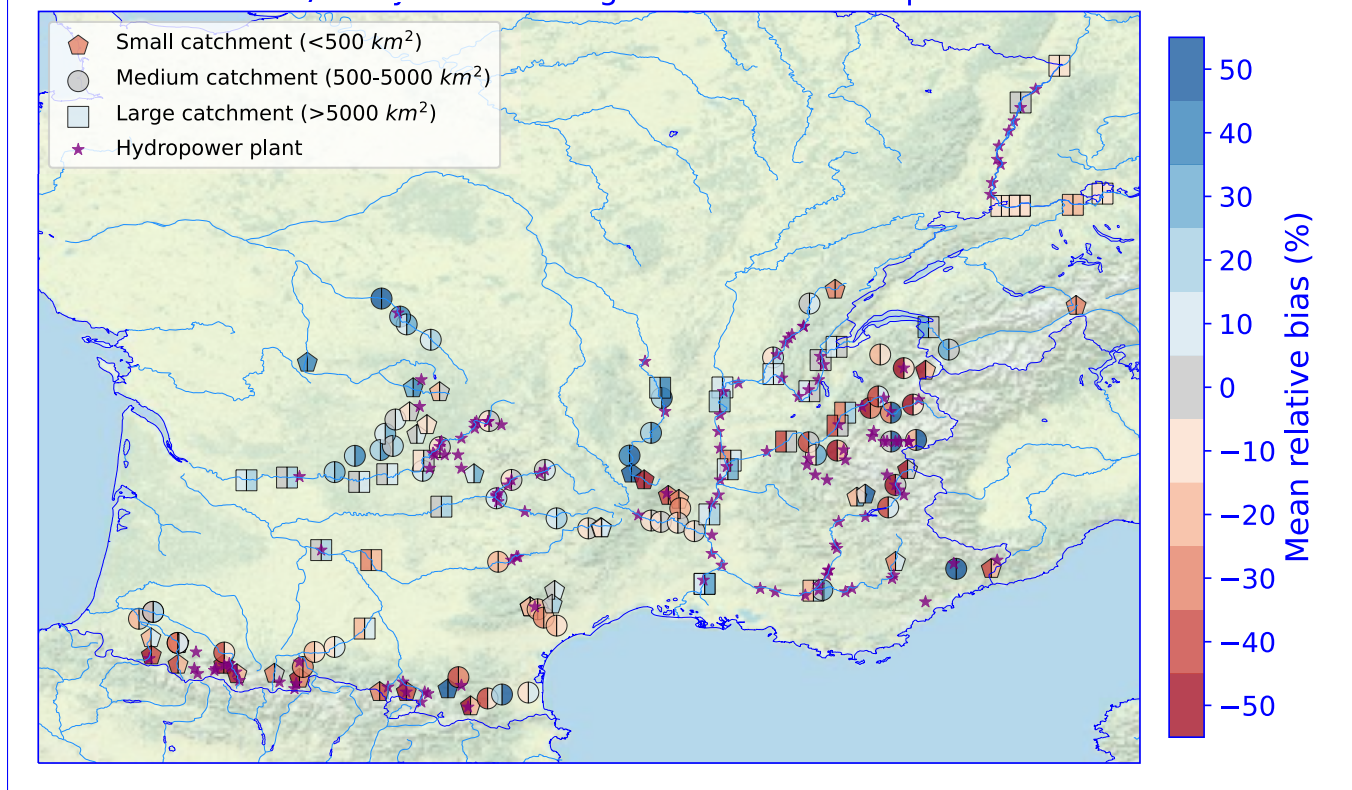


Figure E3. Relative bias of average discharge simulated by ORCHIDEE under alternative forcings for a selection of gauging stations located on French rivers equipped for hydropower for the period 2010-2020. The left coloring indicated the average bias of discharges simulated under SAF_COM while the right coloring indicated the average bias of simulations under SAF_SPAZM.

Source: authors, based on a layer by U.S. National Park Service

seasonality can be attributed to the non-representation of Lemman reservoir management in our model, which is known to play a crucial role in shaping discharge seasonality in the upper Rhone (Habets et al., 1999).

1090 Poundage plants are distributed across various catchments. Some of them are concentrated in the upper Dordogne river, notably the Chastang plant, the most powerful poundage facility, which benefits from a gauging station at its location. We find a positive NSE for this station, indicating that the seasonality is well captured by the model.

1095 Finally, some run-of-river and poundage plants are also concentrated in the Alps, where we focus on two gauging stations: Chamonix, situated in a small upper catchment, close to a run-of-river plant and Cheylas, positioned on a large river (l'Isère), downstream from several power plants. At Chamonix, we find a seasonal bias as the model simulates an earlier discharge peak compared to observations (around 2 months ahead). At Cheylas, the model overestimates the seasonal variability of the

discharge, with higher flows during Spring and lower flows during Winter, which can be attributed - at least in part - to the non-representation of reservoir management at this stage of our study (see Sect. 4.2).

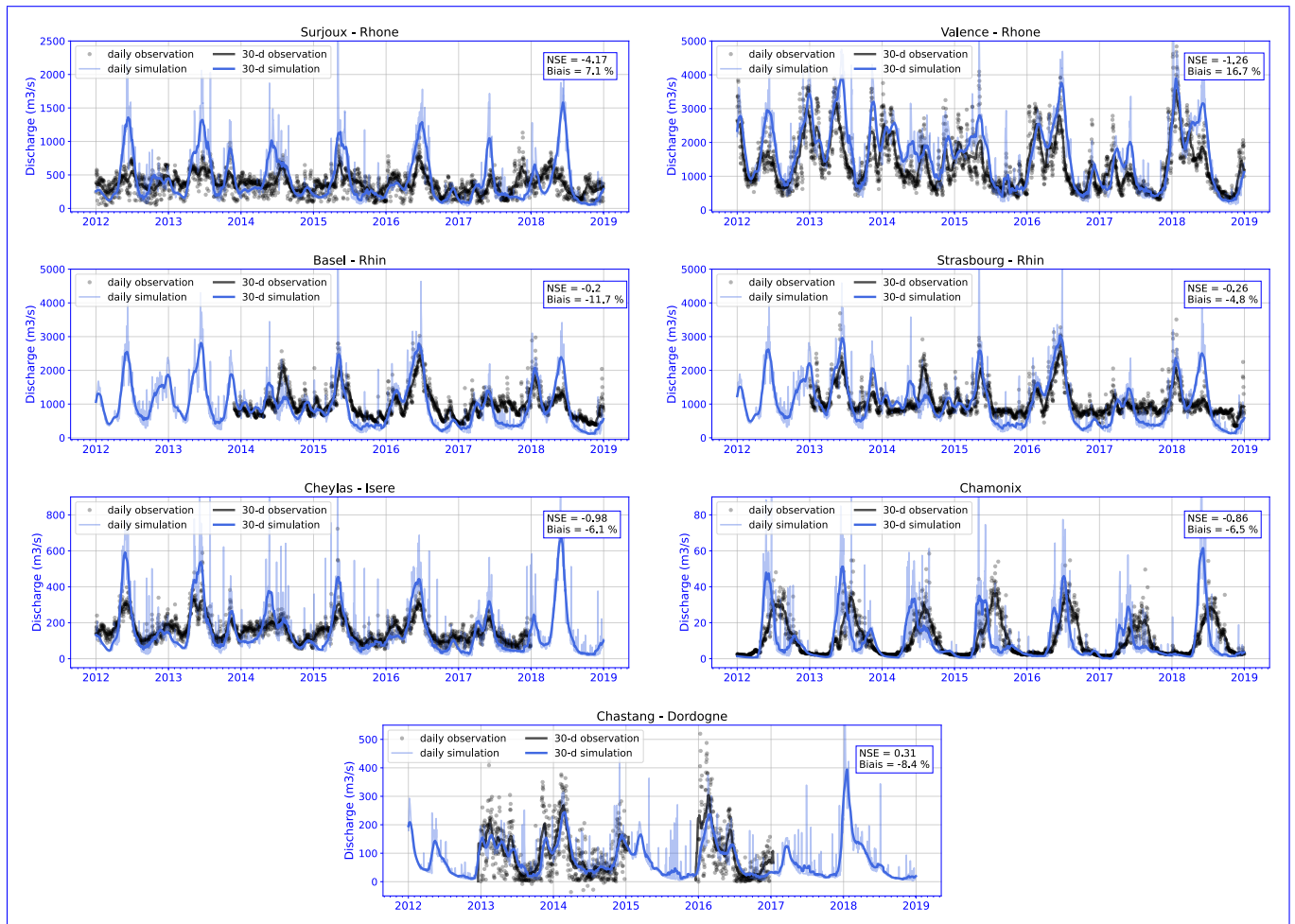


Figure E4. HTUs representation in the model Comparison of simulated and observed river discharges for the same spatial area as Figure D1 at a selection of gauging stations. The location of hydropower infrastructures is selected stations are indicated in Figure E1. Fines lines and dots are daily time series while ticker lines are 30-day sliding averages. NSE metrics are computed on a daily time series.

Author contributions. LB developed the code, designed and executed the numerical evaluations, and wrote the first draft of the manuscript. JP, PD and PQ supervised the study. All authors jointly discussed the methodology, interpreted the results and improved the manuscript.

1100 *Competing interests.* The authors declare that they have no conflict of interest.

Acknowledgements. Baratgin's PhD is supported by the French Ministry of Agriculture. The authors are grateful to EDF-DTG for providing the SPAZM precipitation data and to Meteo-France for providing SAFRAN and COMEPHORE data. HydroPortail and ODRÉ are thanked for collecting and distributing respectively the discharge and power production data. IPSL's MesoCentre is thanked for the computer time.

References

- 1105 Abeshu, G. W., Tian, F., Wild, T., Zhao, M., Turner, S., Chowdhury, A., Vernon, C. R., Hu, H., Zhuang, Y., Hejazi, M., et al.: Enhancing the representation of water management in global hydrological models, *Geoscientific Model Development Discussions*, pp. 1–41, 2023.
- Ambec, S. and Doucet, J. A.: Decentralizing hydro power production, *Canadian Journal of Economics/Revue canadienne d'économie*, 36, 587–607, 2003.
- Birman, C., Karbou, F., Mahfouf, J.-F., Lafaysse, M., Durand, Y., Giraud, G., Mérindol, L., and Hermozo, L.: Precipitation analysis over the French Alps using a variational approach and study of potential added value of ground-based radar observations, *Journal of Hydrometeorology*, 18, 1425–1451, 2017.
- 1110 CFBR: Les barrages en France, <https://www.barrages-cfbr.eu/-En-France->, 2021.
- Chowdhury, A. K., Dang, T. D., Nguyen, H. T., Koh, R., and Galelli, S.: The Greater Mekong's climate-water-energy nexus: How ENSO-triggered regional droughts affect power supply and CO2 emissions, *Earth's Future*, 9, e2020EF001 814, 2021.
- 1115 Dang, T. D., Chowdhury, A. K., and Galelli, S.: On the representation of water reservoir storage and operations in large-scale hydrological models: implications on model parameterization and climate change impact assessments, *Hydrology and Earth System Sciences*, 24, 397–416, 2020.
- European Commission and Joint Research Centre (JRC): JRC Hydro-power database, <http://data.europa.eu/89h/52b00441-d3e0-44e0-8281-fda86a63546d>, 2019.
- 1120 Fekete, B. M., Wisser, D., Kroeze, C., Mayorga, E., Bouwman, L., Wollheim, W. M., and Vörösmarty, C.: Millennium ecosystem assessment scenario drivers (1970–2050): climate and hydrological alterations, *Global Biogeochemical Cycles*, 24, 2010.
- François, B.: Gestion optimale d'un réservoir hydraulique multiusages et changement climatique. Modèles, projections et incertitudes: Application à la réserve de Serre-Ponçon, Ph.D. thesis, Université de Grenoble, 2013.
- Fumière, Q., Déqué, M., Nuissier, O., Somot, S., Alias, A., Caillaud, C., Laurantin, O., and Seity, Y.: Extreme rainfall in Mediterranean France during the fall: added value of the CNRM-AROME Convection-Permitting Regional Climate Model, *Climate Dynamics*, 55, 77–91, 2020.
- 1125 Gottardi, F., Obled, C., Gailhard, J., and Paquet, E.: Régionalisation des précipitations sur les massifs montagneux français à l'aide de régressions locales et par types de temps, *Climatologie*, 5, 7–25, 2008.
- Habets, F., Etchevers, P., Golaz, C., Leblois, E., Ledoux, E., Martin, E., Noilhan, J., and Ottlé, C.: Simulation of the water budget and the river flows of the Rhone basin, *Journal of Geophysical Research: Atmospheres*, 104, 31 145–31 172, 1999.
- 1130 Haddeland, I., Skaugen, T., and Lettenmaier, D. P.: Anthropogenic impacts on continental surface water fluxes, *Geophysical Research Letters*, 33, 2006.
- Hanasaki, N., Kanae, S., and Oki, T.: A reservoir operation scheme for global river routing models, *Journal of Hydrology*, 327, 22–41, 2006.
- IEA: Hydropower Special Market Report, Tech. rep., IEA, <https://www.iea.org/reports/hydropower-special-market-report>, 2021.
- 1135 Krinner, G., Viovy, N., de Noblet-Ducoudré, N., Ogée, J., Polcher, J., Friedlingstein, P., Ciais, P., Sitch, S., and Prentice, I. C.: A dynamic global vegetation model for studies of the coupled atmosphere-biosphere system, *Global Biogeochemical Cycles*, 19, 2005.
- Lehner, B., Czisch, G., and Vassolo, S.: The impact of global change on the hydropower potential of Europe: a model-based analysis, *Energy Policy*, 33, 839–855, 2005.

- 1140 Lehner, B., Liermann, C. R., Revenga, C., Vörösmarty, C., Fekete, B., Crouzet, P., Döll, P., Endejan, M., Frenken, K., Magome, J., et al.: High-resolution mapping of the world's reservoirs and dams for sustainable river-flow management, *Frontiers in Ecology and the Environment*, 9, 494–502, 2011.
- Liu, X., Tang, Q., Voisin, N., and Cui, H.: Projected impacts of climate change on hydropower potential in China, *Hydrology and Earth System Sciences*, 20, 3343–3359, 2016.
- 1145 Lund, J. R. and Guzman, J.: Derived operating rules for reservoirs in series or in parallel, *Journal of water resources planning and management*, 125, 143–153, 1999.
- Magand, C., Ducharne, A., Tilmant, F., Le Moine, N., Sauquet, E., Mathevet, T., Vidal, J.-P., and Perrin, C.: Hybridation de réanalyses météorologiques de surface pour les zones de montagne: exemple du produit DuO sur le bassin de la Durance, *La Houille Blanche*, pp. 77–85, 2018.
- Nazemi, A. and Wheeler, H. S.: On inclusion of water resource management in Earth system models, Part 1: Problem definition and representation of water demand, *Hydrology and Earth System Sciences*, 19, 33–61, <https://doi.org/10.5194/hess-19-33-2015>, 2015a.
- 1150 Nazemi, A. and Wheeler, H. S.: On inclusion of water resource management in Earth system models, Part 2: Representation of water supply and allocation and opportunities for improved modeling, *Hydrology and Earth System Sciences*, 19, 63–90, <https://doi.org/10.5194/hess-19-63-2015>, 2015b.
- Neverre, N.: Rareté de l'eau et relations interbassins en Méditerranée sous changements globaux. Développement et application d'un modèle hydroéconomique à large échelle, Ph.D. thesis, Université Paris-Saclay (ComUE), 2015.
- Nguyen-Quang, T., Polcher, J., Ducharne, A., Arsouze, T., Zhou, X., Schneider, A., and Fita, L.: ORCHIDEE-ROUTING: revising the river routing scheme using a high-resolution hydrological database, *Geoscientific Model Development*, 11, 4965–4985, 2018.
- ODRÉ: Registre 2015 des installations de production raccordées au réseau de transport d'électricité, <https://www.data.gouv.fr/fr/datasets/registre-2015-des-installations-de-production-racordees-au-reseau-de-transport-deelectricite/>, 2015.
- 1160 ODRÉ: Registre 2016 des installations de production raccordées au réseau de transport d'électricité, <https://www.data.gouv.fr/fr/datasets/registre-2016-des-installations-de-production-racordees-au-reseau-de-transport-deelectricite/>, 2016.
- ODRÉ: Registre national des installations de production et de stockage d'électricité (au 31 décembre 2018), <https://www.data.gouv.fr/fr/datasets/registre-national-des-installations-de-production-et-de-stockage-deelectricite-au-31-decembre-2018/>, 2018.
- Oikonomou, K., Tarroja, B., Kern, J., and Voisin, N.: Core process representation in power system operational models: Gaps, challenges, and 1165 opportunities for multisector dynamics research, *Energy*, 238, 122 049, 2022.
- Polcher, J., Schrapffer, A., Dupont, E., Rinchiuso, L., Zhou, X., Boucher, O., Mouche, E., Ottlé, C., and Servonnat, J.: Hydrological modelling on atmospheric grids; using graphs of sub-grid elements to transport energy and water, *EGUsphere*, pp. 1–34, 2023.
- Quintana-Segui, P., Le Moigne, P., Durand, Y., Martin, E., Habets, F., Baillon, M., Canellas, C., Franchisteguy, L., and Morel, S.: Analysis of near-surface atmospheric variables: Validation of the SAFRAN analysis over France, *Journal of applied meteorology and climatology*, 1170 47, 92–107, 2008.
- Ralston Fonseca, F., Craig, M., Jaramillo, P., Bergés, M., Severnini, E., Loew, A., Zhai, H., Cheng, Y., Nijssen, B., Voisin, N., et al.: Effects of climate change on capacity expansion decisions of an electricity generation fleet in the Southeast US, *Environmental Science & Technology*, 55, 2522–2531, 2021.
- Reynolds, C., Jackson, T., and Rawls, W.: Estimating soil water-holding capacities by linking the Food and Agriculture Organization soil 1175 map of the world with global pedon databases and continuous pedotransfer functions, *Water Resources Research*, 36, 3653–3662, 2000.

- RTE: Generated power aggregated by sector, https://www.services-rte.com/en/download-data-published-by-rte.html?category=generation&type=actual_generations_per_production_type, a.
- RTE: Generated power aggregated by unit, https://www.services-rte.com/en/download-data-published-by-rte.html?category=generation&type=actual_generations_per_unit, b.
- 1180 RTE: Hydraulic stock, https://www.services-rte.com/en/download-data-published-by-rte.html?category=generation&type=water_reserves, c.
- RTE, Syndicat des Energies Renouvelables, ENEDIS, ADEeF, and Agence ORE: Panorama de l'électricité renouvelable en 2016, <https://www.actu-environnement.com/media/pdf/news-28448-panorama-electricite-renouvelable-pour-annee-2016.pdf>, 2016.
- RTE, Syndicat des Energies Renouvelables, ENEDIS, ADEeF, and Agence ORE: Panorama de l'électricité renouvelable en 2018, https://assets.rte-france.com/prod/public/2020-06/Panorama%20de%20l%27%C3%A9lectricit%C3%A9%20renouvelable%20au%2031%20decembre%202018_compressed.pdf, 2018.
- Schapi: HydroPortail, <https://hydro.eaufrance.fr/>, 2022.
- Siala, K., Chowdhury, A. K., Dang, T. D., and Galelli, S.: Solar energy and regional coordination as a feasible alternative to large hydropower in Southeast Asia, *Nature Communications*, 12, 4159, 2021.
- 1190 Sterl, S., Vanderkelen, I., Chawanda, C. J., Russo, D., Brecha, R. J., Van Griensven, A., van Lipzig, N. P., and Thiery, W.: Smart renewable electricity portfolios in West Africa, *Nature sustainability*, 3, 710–719, 2020.
- Stoft, S.: *Power system economics: designing markets for electricity*, vol. 468, IEEE press Piscataway, 2002.
- Tabary, P., Dupuy, P., L'Henaff, G., Gueguen, C., Moulin, L., and Laurentin, O.: A 10-year (1997–2006) reanalysis of Quantitative Precipitation Estimation over France: methodology and first results, IAHS-AISH publication, pp. 255–260, 2012.
- 1195 Turner, S. W. and Voisin, N.: Simulation of hydropower at subcontinental to global scales: a state-of-the-art review, *Environmental Research Letters*, 2022.
- Turner, S. W., Ng, J. Y., and Galelli, S.: Examining global electricity supply vulnerability to climate change using a high-fidelity hydropower dam model, *Science of the Total Environment*, 590, 663–675, 2017.
- Van Vliet, M. T., Vögele, S., and Rübberke, D.: Water constraints on European power supply under climate change: impacts on electricity prices, *Environmental Research Letters*, 8, 035 010, 2013.
- 1200 Van Vliet, M. T., Wiberg, D., Leduc, S., and Riahi, K.: Power-generation system vulnerability and adaptation to changes in climate and water resources, *Nature Climate Change*, 6, 375–380, 2016.
- Voisin, N., Dyreson, A., Fu, T., O'Connell, M., Turner, S. W., Zhou, T., and Macknick, J.: Impact of climate change on water availability and its propagation through the Western US power grid, *Applied Energy*, 276, 115 467, 2020.
- 1205 Wagner, T., Themeßl, M., Schüppel, A., Gobiet, A., Stigler, H., and Birk, S.: Impacts of climate change on stream flow and hydro power generation in the Alpine region, *Environmental Earth Sciences*, 76, 1–22, 2017.
- Wessel, M., Madlener, R., and Hilgers, C.: Economic feasibility of semi-underground pumped storage hydropower plants in open-pit mines, *Energies*, 13, 4178, 2020.
- Wood, A. J., Wollenberg, B. F., and Sheblé, G. B.: *Power generation, operation, and control*, John Wiley & Sons, 2013.
- 1210 Yamazaki, D. I., Jeison, S., Paul, D. B., George, H. A., and Tamlin, M. P.: MERIT Hydro: A high-resolution global hydrography map based on latest topography datasets, *Water Resources Research*, 55, 5053–5073, 2019.
- Zhou, T., Voisin, N., and Fu, T.: Non-stationary hydropower generation projections constrained by environmental and electricity grid operations over the western United States, *Environmental Research Letters*, 13, 074 035, 2018.

Zhou, X., Polcher, J., and Dumas, P.: Representing human water management in a land surface model using a supply/demand approach, 1215 Water Resources Research, 57, e2020WR028 133, 2021.